Chapter 17

Late Pleistocene Mountain Glaciation in the Lake Bonneville Basin

B.J.C. Laabs* and J.S. Munroe†
*North Dakota State University, Fargo, ND, United States
†Middlebury College, Middlebury, VT, United States

ABSTRACT

The record of the last Pleistocene glaciation in the Lake Bonneville basin has been known for decades and has improved significantly due to expanded mapping and geologic dating efforts. Although ice occupied only a small portion of the basin and constituted a small component of the lake water budget, the pattern of glaciation in space and time can be combined with the stratigraphic record from Lake Bonneville to improve the understanding of regional climate change during and after the last glaciation. Mountain glaciers were most abundant in the eastern/Rocky Mountain sector of the basin, with the vast majority of ice volume concentrated in the Wasatch and Uinta Mountains. Here, the geomorphic record of the last glaciation is well preserved, stratigraphic observations of sediments of Lake Bonneville and valley glaciers are documented, and cosmogenic ^{10}Be exposure ages of several moraines based on new production models of in situ ^{10}Be are reported. Terminal moraines here, and in the western sector of the basin, were occupied near the time of the Bonneville highstand at 18 ka and subsequently abandoned while the lake continued to overflow. This constitutes a significant revision to initial reports of ^{10}Be exposure ages based on earlier production rate models, which suggest that ice retreat corresponded to the fall of Lake Bonneville from the Provo shoreline. Still, temporal correspondence of the Lake Bonneville highstand and glacier maxima support the previously proposed model that climate during the lake highstand was favorable for maxima of both glaciers and lakes. The onset of ice retreat while the lake overflowed, however, suggests warming in the basin at c.18 ka but with sufficient precipitation to sustain a positive water budget of Lake Bonneville.

Keywords: Lake Bonneville, Mountain glaciation, Cosmogenic exposure dating, Pleistocene climate change

Developments in Earth Surface Processes, Vol. 20. http://dx.doi.org/10.1016/B978-0-444-63590-7.00017-2

17.1 INTRODUCTION

During the last Pleistocene glaciation, mountain glaciers were present in 15 separate mountain ranges within the hydrologic basin of Lake Bonneville (Osborn and Bevis, 2001; Fig. 17.1). The vast majority of this total ice volume

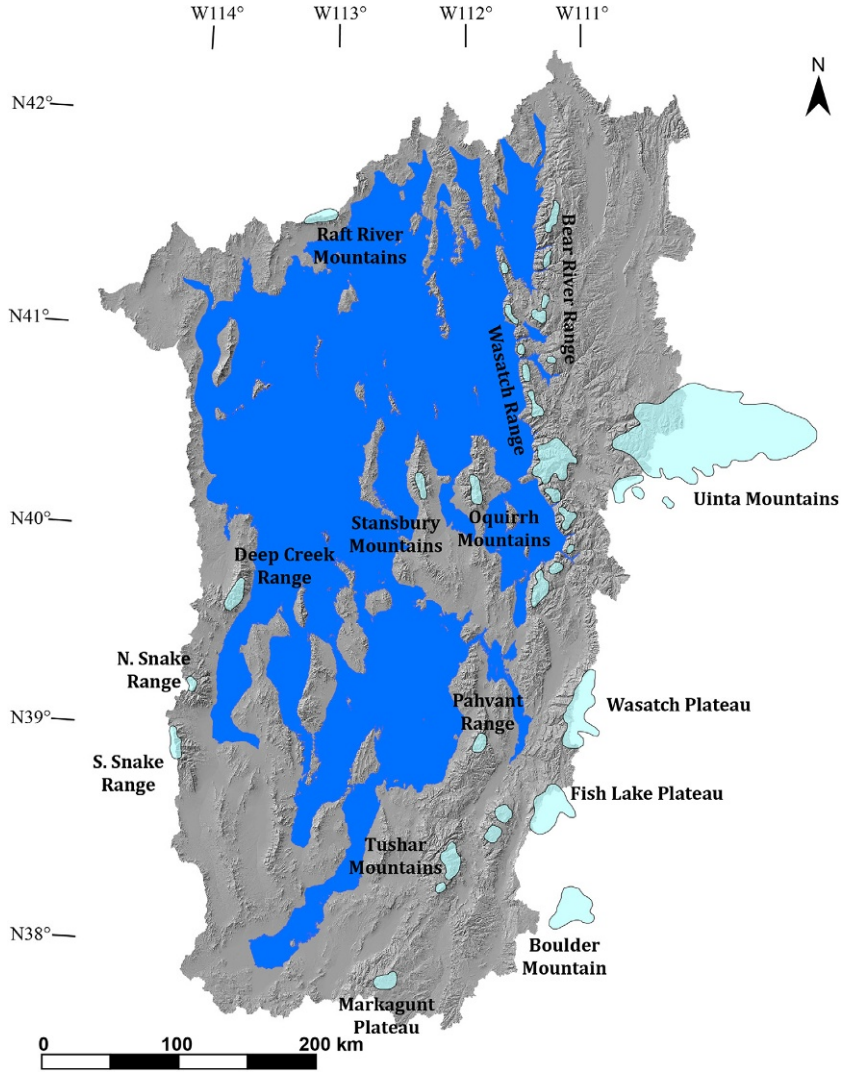

FIG. 17.1 Shaded-relief map of the Lake Bonneville basin produced from a mosaic of 30-m digital elevation models from the National Elevation Dataset (http://ned.usgs.gov). The maximum extent of Lake Bonneville is shown in *blue* (modified from http://gis.utah.gov) and Pleistocene mountain glacier systems in the basin are transparent *light blue*. *Modified from Biek, R., Willis, G., Ehler, B., 2010. Utah's Glacial Geology. Utah Geol. Surv. Notes, 42(3), 1–4.*

was concentrated in two ranges east of Lake Bonneville, the Wasatch and Uinta Mountains of northeastern Utah (Munroe and Laabs, 2009). These two ranges have been the focus of detailed glacial mapping efforts (eg, McCoy, 1977; Scott and Shroba, 1985; Personius and Scott, 1992; Laabs and Carson, 2005; Munroe, 2005; Refsnider et al., 2007; Laabs et al., 2011), which have supported reconstruction of glacier extent as well as the development of local cosmogenic ^{10}Be chronologies for the last glaciation (Munroe et al., 2006; Laabs et al., 2009; Laabs et al., 2011). These and other studies of the pattern of mountain glaciation in the Lake Bonneville basin, hereafter the "LBB" (eg, Munroe and Mickelson, 2002; Munroe et al., 2006), along with neighboring settings (Osborn and Bevis, 2001; Marchetti, 2007) have led to models for climatic and hydrologic conditions accompanying the glacier maxima, subsequent retreat, and the highstand of Lake Bonneville. Although mountain ice was likely a minor component of the total hydrologic budget of the lake (Fig. 17.2), documenting the spatial and temporal pattern of glaciation in the LBB provides a critical framework for understanding climatic changes during the last pluvial cycle.

Glacial deposits in the region surrounding Lake Bonneville were recognized by Gilbert (1890) and first documented by Atwood (1909) in the Wasatch and Uinta Mountains and by Blackwelder (1931) in northern ranges of the LBB. These studies interpreted the glacial deposits to represent at least two Pleistocene glaciations, with older glaciations being generally more extensive than later episodes. In the Wasatch and Uinta Mountains, the

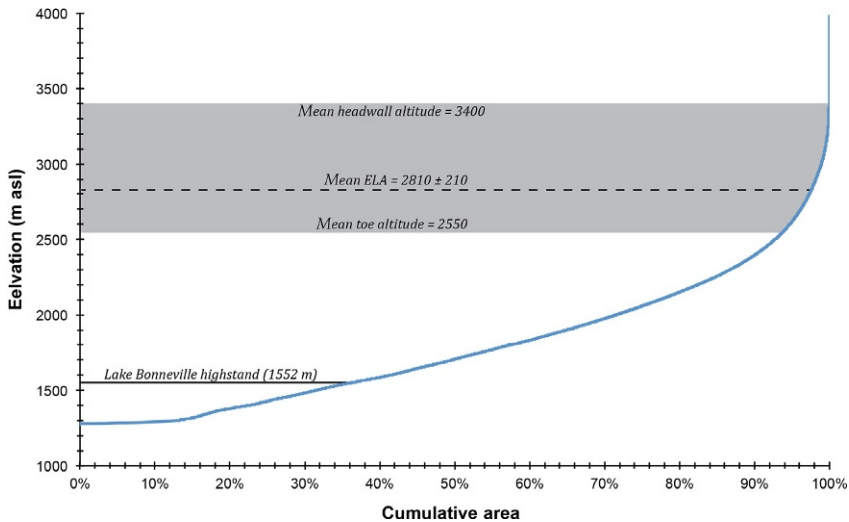

FIG. 17.2 Hypsometry of the Lake Bonneville basin. *Gray area* indicates the mean elevation range and equilibrium-line altitude (ELA) of reconstructed late Pleistocene glaciers listed in Table 17.2.

mapping of Atwood (1909) was succeeded by larger-scale mapping of glacial deposits by Bradley (1936), Richmond (1964), Osborn (1973), Scott and Shroba (1985), Bryant (1992), Personius and Scott (1992), Oviatt (1994), Munroe (2005), Laabs and Carson (2005), Refsnider et al. (2007), and Munroe and Laabs (2009) among others. Although glacial deposits are generally restricted to the mountain headwaters of the LBB, Madsen and Currey (1979), Scott (1988), and Godsey et al. (2005) documented stratigraphic relationships between glacial till and nearshore deposits of Lake Bonneville along the western front of the Wasatch Mountains near the mouths of Little Cottonwood and Bells Canyons. Although G.K. Gilbert's observations of morphological relationships of glacial and lacustrine deposits concluded correctly that glaciers advanced to the western front of the Wasatch Mountains prior to the Lake Bonneville highstand, some of the more recent studies reached a contrasting conclusion (as summarized by Scott, 1988).

Studies of glacial deposits in the Wasatch and Uinta Mountains, combined with mapping of glacial features in the smaller southeastern (Marchetti, 2007) and western ranges (Osborn and Bevis, 2001; and this study) of the LBB, have helped to reveal the pattern of mountain glaciation during the last glaciation. Despite the small glacial footprint relative to the size of Lake Bonneville (Figs. 17.1 and 17.2), the spatial distribution of ice provides a useful framework for understanding: (1) the range of possible temperature and precipitation changes accompanying the last glaciation in the LBB; and (2) the potential climatic effects that Lake Bonneville may have had on glacier mass balance in neighboring mountains. Previous work described the pattern of glaciation within and beyond the northern sector of the LBB in terms of glacier equilibrium-line altitudes (ELAs; Munroe and Mickelson, 2002; Munroe et al., 2006; Laabs et al., 2011). These studies reveal an intriguing west-to-east trend in ELAs across the northeastern Nevada and Utah (Fig. 17.3), such that ELAs decline nearly 400 m across Lake Bonneville from the Deep Creek–Stansbury–Oquirrh–Wasatch Ranges, and then rise sharply by 400–600 m across the western Uinta Mountains. This pattern is consistent with the hypothesis that Lake Bonneville affected glacier mass balance in downwind mountain ranges, but only if glacier maxima occurred when the lake was present.

In lieu of abundant and clear stratigraphic relationships between glacial and lacustrine deposits in the LBB, understanding the relative timing of moraine occupation and lake highstands relies chiefly on the comparison of radiocarbon-based chronologies of lacustrine deposits of Lake Bonneville (eg, Oviatt, 1997; Reheis et al., 2014; Oviatt, 2015) and cosmogenic chronologies of moraines (eg, Marchetti et al., 2005; Laabs et al., 2009, 2011; Marchetti et al., 2011). Such comparisons have been restricted (prior to this study) to glacial deposits in mountains east and downwind of Lake Bonneville. Broad application of cosmogenic ^{10}Be exposure dating of moraines in the Uinta (Munroe et al., 2006; Refsnider et al., 2008; Laabs et al., 2009)

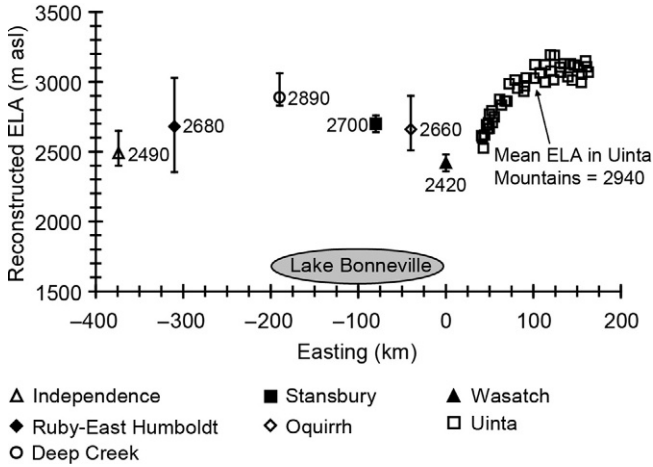

FIG. 17.3 Reconstructed glacier equilibrium-line altitudes (ELAs) across northeastern Nevada and northern Utah. Easting is relative to the eastern shoreline of Lake Bonneville near Salt Lake City, Utah. ELAs indicate the average of the toe-headwall altitude ratio and accumulation–area ratio, as defined in Table 17.1. ELAs for mountains in northeastern Nevada (Ruby–East Humboldt and Independence Ranges) and the eastern Uinta Mountains are from Laabs et al. (2011). *Modified from Laabs, B.J.C., Marchetti, D.W., Munroe, J.S., Refsnider, K.A., Gosse, J.C., Lips, E.W., Becker, R.A., Mickelson, D.M., Singer, B.S., 2011. Chronology of latest Pleistocene mountain glaciation in the western Wasatch Mountains, Utah, U.S.A. Quat. Res. 76, 272–284.*

and Wasatch Mountains (Laabs et al., 2011) has revealed apparent differences in the timing of local glacier maxima. Consistent with stratigraphic observations of Godsey et al. (2005), cosmogenic ^{10}Be exposure ages of moraines in the western Wasatch Mountains reported in these studies indicate that some glaciers persisted at, or readvanced to, their maximum length during the time when Lake Bonneville overflowed (Laabs et al., 2011). In the Uinta Mountains, reported exposure ages of moraines indicate that glaciers in southern and western valleys were at their terminal moraines while Lake Bonneville overflowed, whereas glacial retreat in northern and eastern valleys had begun by this time (Laabs et al., 2009). Although cosmogenic ^{10}Be exposure dating of glacial deposits has helped to establish a framework for reconstructing climate changes accompanying the last glaciation in the LBB, understanding the relative timing of glacier maxima and the rise and fall of Lake Bonneville has been complicated in part by uncertainties in the production of in situ ^{10}Be. A more reliable comparison is now possible due to a local calibration of the in situ production of ^{10}Be directly from geomorphic features constructed by Lake Bonneville (Lifton et al., 2015) and refinements to models of the temporal and spatial scaling of cosmic ray fluxes (Lifton et al., 2014).

The broad goal of this chapter is to describe the pattern of mountain glaciation in the LBB. This is achieved through compilation and review of the available mapping of glacial deposits and landforms in mountain ranges that

hosted glaciers. Because the majority of glacier ice was concentrated in the Wasatch and Uinta Mountains, the spatial pattern of the last glaciation in these two regions is emphasized over other, smaller mountains. The temporal pattern of glaciation is reconsidered here through calculation of previously published and new cosmogenic ^{10}Be exposure ages of moraines in the LBB using the aforementioned refinements to the in situ production rate models by Lifton et al. (2014, 2015), and comparison of these ages to the chronology of Lake Bonneville as described by Oviatt (2015). Again, emphasis is given to the extensively glaciated Wasatch and Uinta Mountains, where the chronology of glacial deposits is known from cosmogenic ^{10}Be exposure dating of moraines. Lastly, previous and new inferences of the climatic and hydrologic relationship of Lake Bonneville and glaciers in neighboring mountains are discussed in the context of existing models of climate change in the southwestern United States during the last glaciation.

17.2 THE PATTERN OF PLEISTOCENE GLACIATION

This section describes the known distribution of glacial deposits and landforms in the glaciated mountain ranges of the LBB, based chiefly on recent 1:24,000-scale field mapping and interpretations of aerial photography. Reconstructions of the aerial and vertical extent of ice presented in numerous figures later are based on this mapping and represented in terms of ice area, volume, and ELA in Table 17.1. For specific information regarding the mapping of glacial deposits, the reader is referred to maps and other documents cited later.

17.2.1 The Wasatch Mountains

A product of late Cenozoic normal faulting at the junction of the Basin and Range and the Middle Rocky Mountains, the Wasatch Mountains are a north–south trending range forming a steep orographic barrier east of Lake Bonneville. The northern segment of the mountain range east of Salt Lake City and Provo features many of the highest summits of the range (eg, Mt. Timpanogos, 3582 m asl) and was the most heavily glaciated part of the range, with the largest glaciers occupying east-to-west flowing valleys (Fig. 17.4). Other segments of the range occupied by ice include a small number of valleys east of Ogden, valleys in the Bear River Range east of Logan (Reheis et al., 2005), and a small number of valleys east and southeast of Provo (Fig. 17.1). The clearest geomorphic indicators of Pleistocene glaciation are classic, mountain glacial–erosional landforms, such as cirques, arêtes, and broad U-shaped valleys (Atwood, 1909; Richmond, 1964). Throughout the Wasatch Mountains, glacial sediment is sparsely preserved within canyons (Richmond, 1964; McCoy, 1977), likely due to postglacial modification of glacial valleys. The best-preserved deposits of till and outwash are located

TABLE 17.1 Reconstructed Glacier Area, Volume, and Equilibrium-Line Altitudes in the Lake Bonneville Basin

Number	Mountains[a]	Drainage	Area (km^2)	Volume (km^3)[b]	ELA—Toe-Headwall Altitude Ratio[c] (m asl)	ELA—Accumulation-Area Ratio[d] (m asl)	Mean ELA (m asl)	1σ
1	South Snake	Blue Canyon	0.7	0.02	3133	3135	3134	1
2		Bald Mtn East	0.2	0.00	3110	3087	3098	16
3		Bald Mtn West	1.1	0.04	3063	3033	3048	22
4		Lehman Creek	10.8	1.12	2997	3083	3040	61
5		Baker Creek	5.5	0.42	3147	3080	3114	48
6		Snake Creek North	1.8	0.08	3114	3097	3105	12
7		Snake Creek Middle	2.2	0.11	3078	3018	3048	43
8		Snake Creek South	0.7	0.02	3162	3251	3207	63
9		Williams Canyon	1.0	0.04	3063	3056	3059	5
10		Big Canyon	0.9	0.03	3140	3110	3125	22
		Sum	*24.9*	*1.9*		*Rangewide mean ELA*	*3098*	*52*
11	Deep Creek[e]	Haystack Peak	1.7	0.08	3021	3170	3096	105
12		Red Cedar Creek	3.1	0.18	2951	3206	3079	181
13		Steves Creek North	0.6	0.02	2793	2804	2798	8
14		Steves Creek South	0.7	0.02	2834	2816	2825	13

15		Granite Creek	0.7	0.02	3078	3194	3136	82
		Sum	*6.8*	*0.3*		*Rangewide mean ELA*	*2987*	*161*
16	Stansbury[e]	Pass Canyon	0.4	0.01	2570	2606	2588	26
17		Little Pole Canyon	0.4	0.01	2692	2719	2705	19
18		North Willow	1.0	0.03	2488	2597	2542	77
19		Big Pole Canyon	0.8	0.02	2732	2658	2695	52
20		Mining fork	2.1	0.10	2441	2560	2500	85
21		Spring Canyon	0.6	0.02	2713	2719	2716	4
22		South Willow Canyon	5.2	0.39	2422	2606	2514	130
23		Big Creek Canyon	1.3	0.05	2692	2707	2699	10
		Sum	*11.8*	*0.6*		*Rangewide mean ELA*	*2620*	*93*
24	Fish Lake Plateau[f]	Jorgensen Creek North	0.5	0.01	3035	3020	3028	11
25		Jorgensen Creek South	0.9	0.03	3020	2980	3000	28
26		Seven Mile	3.5	0.22	3060	2950	3005	78
27		Rock Canyon	2.1	0.10	3165	3130	3148	25
28		Pelican Canyon	4.2	0.28	3030	3190	3110	113
29		Tasha Creek	11.3	1.20	3020	3130	3075	78
		Sum	*22.5*	*1.8*		*Rangewide mean ELA*	*3061*	*60*

Continued

TABLE 17.1 Reconstructed Glacier Area, Volume, and Equilibrium-Line Altitudes in the Lake Bonneville Basin—Cont'd

Number	Mountains	Drainage	Area (km^2)	Volume (km^3)	ELA—Toe-Headwall Altitude Ratio (m asl)	ELA—Accumulation-Area Ratio (m asl)	Mean ELA (m asl)	1σ
30	Oquirrh[e]	Settlement Canyon	1.0	0.03	2750	2804	2777	38
31		Lowe Canyon	0.7	0.02	2654	2658	2656	3
32		Jackson Hollow	0.5	0.01	2675	2755	2715	57
33		Jumpoff	2.2	0.11	2590	2606	2598	11
		Sum	*4.4*	*0.2*		*Rangewide mean ELA*	*2686*	*77*
34	Wasatch[e]	American Fork	20.5	2.86	2567	2560	2564	5
35		Little Cottonwood	42.2	8.35	2141	2606	2374	329
36		Bells	7.2	0.61	2221	2713	2467	348
37		Silver Lake	8.4	0.77	2610	2682	2646	51
38		Dry Creek	15.1	1.83	2226	2652	2439	301
		Sum	*93.3*	*14.43*		*Rangewide mean ELA*	*2498*	*107*
39	Uinta[e]	Heber Mountain	0.9	0.03	2403	2469	2436	47
40		Pinon Canyon	0.5	0.01	2610	2621	2616	8
41		Swifts Canyon	2.1	0.10	2520	2682	2601	115
42		Bear Basin	0.8	0.03	2524	2524	2524	0

43		Mill Fork	8.8	0.83	2570	2667	2619	69
44		South Fork	17.5	2.28	2610	2774	2692	116
45		Nobletts Creek	2.0	0.10	2680	2646	2663	24
46		Shingle Mil	1.6	0.07	2670	2743	2707	52
47		Shingle Mill East	0.3	0.01	2700	2633	2667	47
48		Bear Trap North	0.3	0.01	2770	2768	2769	1
49		Smith & Morehouse	125.0	41.83	2710	2880	2795	120
50		Slader Ridge West	0.4	0.01	2700	2719	2710	13
51		Broad Canyon	1.3	0.05	2800	2725	2763	53
52		Slader Creek	2.5	0.13	2770	2728	2749	30
53		Weber River	125.0	41.83	2780	2972	2876	136
54		Shingle Creek	16.6	2.11	2663	2902	2783	169
55		Coop Creek	7.8	0.69	2642	2793	2718	107
56		Yellow Pine Creek	5.6	0.43	2598	2744	2671	103
57		South Fork Weber	17.5	2.28	2774	2610	2692	116
58		West Fork Bear River	47.9	10.07	2788	2880	2834	65
59		Chalk Creek	5.0	0.36	2888	2840	2864	34
60		Provo River	132.7	45.72	2835	2950	2893	81

Continued

TABLE 17.1 Reconstructed Glacier Area, Volume, and Equilibrium-Line Altitudes in the Lake Bonneville Basin—Cont'd

Number	Mountains	Drainage	Area (km^2)	Volume (km^3)	ELA—Toe-Headwall Altitude Ratio (m asl)	ELA—Accumulation-Area Ratio (m asl)	Mean ELA (m asl)	1σ
61		North Fork Provo	59.5	13.88	2852	2950	2901	69
62		Hayden Fork Bear River	118.7	38.73	2948	3025	2987	54
63		East Fork Bear River	56.7	12.93	2988	3035	3012	33
		Sum	*757.0*	*214.5*		*Mean ELA of Western Uinta Icefield*	*2741*	*136*

Notes: List of glaciers is not exhaustive. Excludes ice in Big Cottonwood Canyon (Wasatch) and numerous small ice masses in valleys of the eastern sector of the basin where ice extents are poorly known.
[a]*Mountain ranges are listed from west to east.*
[b]*Based on area–volume scaling relationship for steady-state glaciers, where* $\log V = \gamma \log A + k$, *where* V, *volume,* A, *surface area,* γ, *1.375 (Bahr et al., 1997) or 1.56 (Radić et al., 2007).*
[c]*Toe-headwall altitude ratio = 0.4 (highest headwall altitude—toe altitude) + toe altitude.*
[d]*Assumed ratio accumulation–area ratio of 0.65.*
[e]*ELAs are from Laabs et al. (2011) and references therein.*
[f]*ELAs and ice area from Marchetti et al. (2011).*

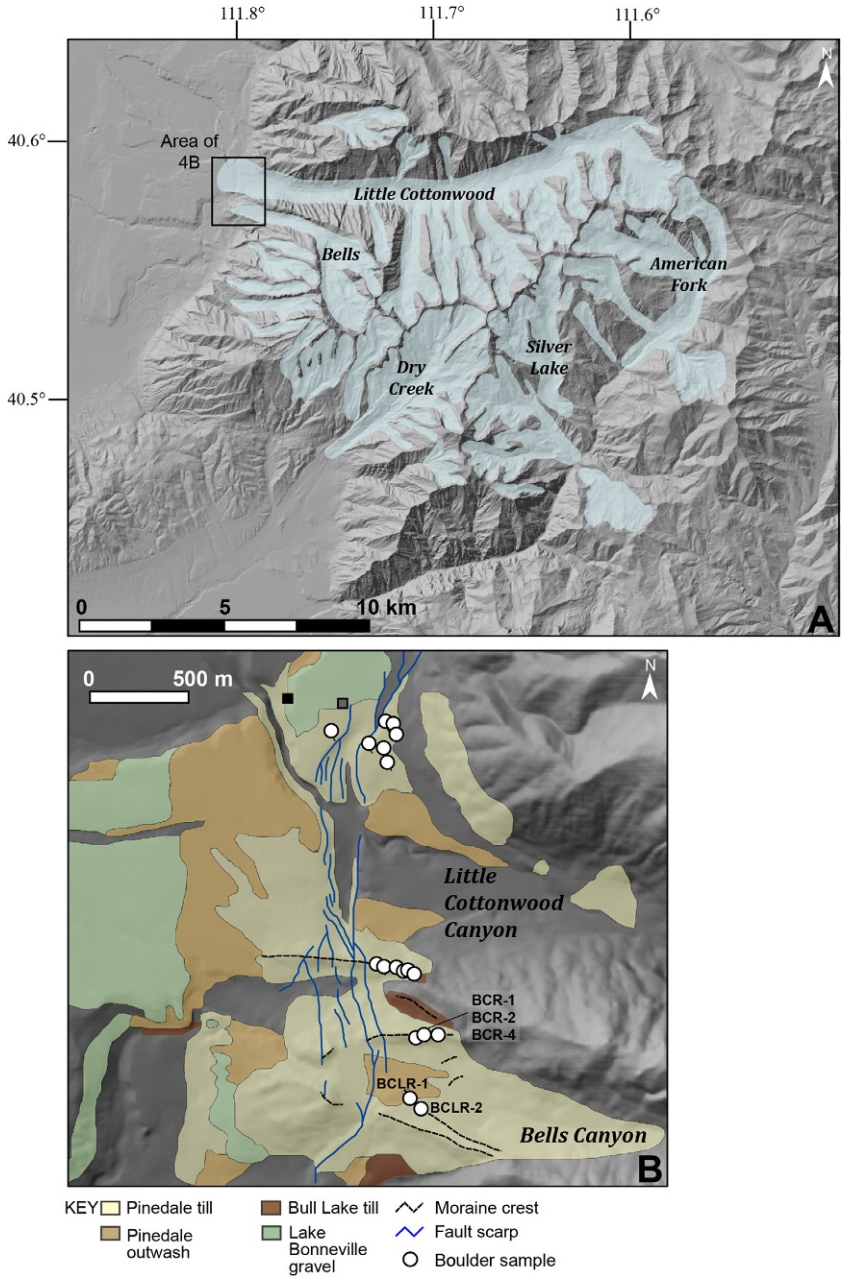

FIG. 17.4 (A) Shaded-relief map of a glaciated portion of the Wasatch Mountains near Salt Lake City, UT (produced from a mosaic of 30-m digital elevation models from the National Elevation Dataset, http://ned.usgs.gov). Pleistocene ice extents are transparent *light blue*. (B) Surficial geologic mapping of Personius and Scott (1992) with *shaded* relief. Boulder locations refer to samples of the terminal and left-lateral moraine at Little Cottonwood Canyon sampled for cosmogenic ^{10}Be exposure dating, and previously unpublished exposure ages of samples from Bells Canyon. *Boxes* indicate locations of outcrops where stratigraphic relationships of Lake Bonneville deposits and glacial till have been documented by Scott (1988; *black box*) and Godsey et al. (2005; *gray box*).

at or near the mountain front in a small number of glacial valleys, including Little Cottonwood, Bells, Dry Creek (Fig. 17.4), and Big Cottonwood Canyons (Quirk et al., 2015).

After the earliest documentation of glacial deposits in the western Wasatch Mountains by Gilbert (1890), Atwood (1909), and Ives (1950), the first 1:24,000-scale mapping of these deposits by Richmond (1964) subdivided Pleistocene till and outwash to represent at least two glacial episodes. The framework for these subdivisions followed terminology for glacial episodes coined by Blackwelder (1915) and later modified by Richmond (1957), wherein the last two episodes are the Bull Lake (penultimate) and Pinedale (last) Glaciations. These were correlated by Richmond (1965) to the Early and Late Wisconsin Glaciations, respectively, representing the last two periods of major global ice advance. The Pinedale Glaciation culminated in the Rocky Mountains and neighboring regions of the western United States during marine oxygen isotope stage 2 (26–14 ka; Lisiecki and Raymo, 2005), and the Bull Lake most likely during stage 6 (167–132 ka; Lisiecki and Raymo, 2005) or possibly later. Based largely on weathering characteristics of boulders and other sediment comprising moraines, Richmond (1964) concluded that deposits at the mouths of Little Cottonwood and Bells Canyons represent the Bull Lake Glaciation in the Wasatch Mountains and that ice did not reach the mountain front during the Pinedale Glaciation. Deposits in this area were remapped by McCoy (1977), who revised Richmond's interpretation and suggested that moraines at the mouth of Little Cottonwood and Bells Canyons were actually deposited during the last glaciation. This Pinedale age designation was confirmed by a reconsideration of soil formation in glacial and other Quaternary deposits near the mouth of Little Cottonwood Canyon (Scott and Shroba, 1985), and by radiocarbon dating of glacial features at the mountain front and within the canyons (Madsen and Currey, 1979).

The first radiocarbon age limits on glacial deposits led Madsen and Currey (1979) to conclude that glaciers in these two canyons began retreating from their terminal moraines prior to the Lake Bonneville highstand. This observation was supported by stratigraphic relationships of till and lacustrine nearshore gravel near the mouth of Little Cottonwood Canyon (Scott and Shroba, 1985; Scott, 1988). Here, till overlain by nearshore gravel displays a weakly developed soil, indicating a brief (centuries or millennia) period of exposure prior to burial by gravel deposited during the Lake Bonneville highstand. Conversely, Godsey et al. (2005) described interfingered till and shoreline deposits of the Lake Bonneville highstand in a separate exposure on the ice-distal side of the terminal moraine at Little Cottonwood Canyon (Fig. 17.4b), suggesting that the highstand and the local glacial maximum were synchronous.

Evaluating stratigraphic relationships of glacial and lacustrine sediment in the western Wasatch Mountains are complicated by the paucity of

observations, and the fact that the exposures displaying clear stratigraphic relationships between till and lacustrine gravel are no longer visible due to urbanization and removal of deposits. Additionally, numerical ages of glacial deposits limit only the time when ice began retreating from moraine crests, not when ice first reached its maximum extent; therefore, ages of subsurface tills observed by Scott and Shroba (1985) and Godsey et al. (2005) in excavations at the mouths of Little Cottonwood and Bells Canyons could be significantly older than tills forming moraine crests dated by cosmogenic ^{10}Be (Laabs et al., 2011). When considered together, stratigraphic relationships between tills and lacustrine deposits of Lake Bonneville suggest that the termini of glaciers in Little Cottonwood and Bells Canyons occupied the mountain front more than once during the last Pleistocene glaciation. If so, glaciers likely extended to the mountain front both before and during the Lake Bonneville highstand at 18.0 ka.

Reconstructed ice extents in valleys where the locations of glacier termini are clearly delimited by moraines (Fig. 17.4) indicate that ELAs in the western Wasatch Mountains were the lowest in the LBB, ranging from 2374 to 2646 m (Table 17.1; Fig. 17.3). As discussed by Laabs et al. (2011), this pattern is not consistent with the distribution of modern precipitation across the northern sector of the LBB. In fact, winter precipitation at 2750 m, the regionally averaged ELA of the last glaciation, is greater in some ranges west of the Wasatch Mountains (eg, the Ruby and East Humboldt Mountains of northeastern Nevada) but the reconstructed ELA of the last glaciation there is higher. This suggests that, given a uniform temperature depression in mountains of the northern LBB, precipitation patterns differed from modern, possibly due to the presence of Lake Bonneville. This possibility is further discussed later.

17.2.2 The Uinta Mountains

The Uinta Mountains, an east–west-trending Laramide uplift in the Middle Rocky Mountains, are the only range in Utah with summits extending above 4000 m asl and were heavily glaciated during the Pleistocene. The range featured a large number of north- and south-flowing discrete valley glaciers as well as the western Uinta Icefield (Oviatt, 1994; Refsnider et al., 2008), which occupied the westernmost valleys of the Uinta Mountains and drained into Lake Bonneville via the Provo, Weber, and Bear Rivers (Refsnider et al., 2008; Munroe and Laabs, 2009; Fig. 17.5). The western Uinta Icefield was the largest single ice mass in the LBB, likely greater than all other ice masses combined in the basin (Table 17.1), even though the southeastern sector of it extended beyond the watershed divide and drained into the Colorado River system. Among glaciated areas of the western United States, the Uinta Mountains are widely known for their unique glacial geomorphology, prominently displayed along the summit ridge (eg, Hansen, 1975). Most glacial valleys in the Uinta Mountains feature broad, compound cirques formed in quartzite

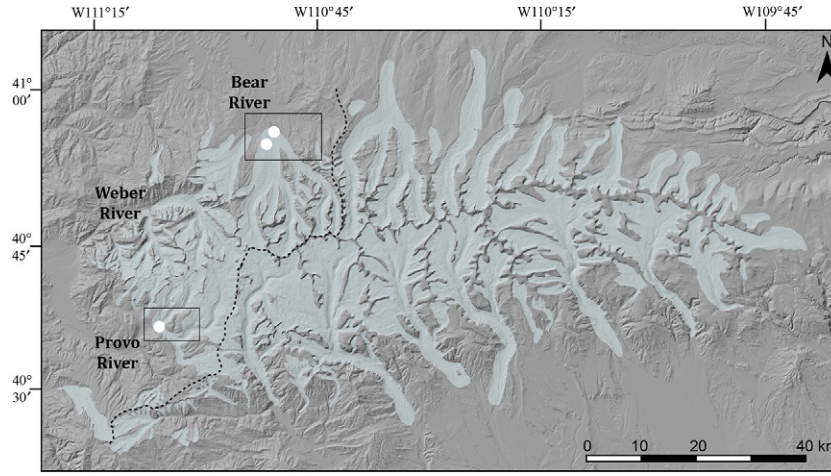

FIG. 17.5 Shaded-relief map of the glaciated portion of the Uinta Mountains (produced from a mosaic of 30-m digital elevation models from the National Elevation Dataset, http://ned.usgs.gov). Pleistocene ice extents are transparent *light blue* (from Munroe and Laabs, 2009). *White circles* indicate locations of moraines with cosmogenic ^{10}Be exposure ages. *Rectangles* indicate areas shown in Fig. 17.6.

and weakly metamorphosed sandstone that were occupied by laterally extensive icefields instead of valley glaciers (Munroe and Laabs, 2009). These icefields drained into one or more large U-shaped valleys that were occupied by valley glaciers extending to the range front. The Western Uinta Icefield is so-named because ice thicknesses were great enough to overwhelm the east–west-trending summit ridge, connecting ice masses on opposite sides of the range (Refsnider et al., 2007; Fig. 17.5).

The earliest mapping of glacial deposits in the Uinta Mountains by Atwood (1909) subdivided well-preserved moraines and outwash into two glacial episodes. These were later termed the Blacks Fork (penultimate) and Smiths Fork (last) Glaciations by Bradley (1936), after sets of well-preserved lateral and terminal moraine complexes in adjacent drainages of the northern Uinta Mountains. Mapping of glacial deposits in the southern Uinta Mountains by Osborn (1973) documented numerous moraine crests interpreted to represent multiple intervals of ice advance and retreat during the last and penultimate glaciations. More recent mapping by Munroe (2005) and Laabs and Carson (2005) subdivided moraines on the basis of soil development (based on soil development indices developed by Douglass, 2000), geometry (height and slope), frequency of large boulders, and morphological relationships with outwash terraces, confirming the extent of the last glaciation in the Uinta Mountains (Fig. 17.5).

Mapping of glacial deposits at 1:24,000-scale greatly expanded the understanding of the extent of the last glaciation in the headwaters of the Provo,

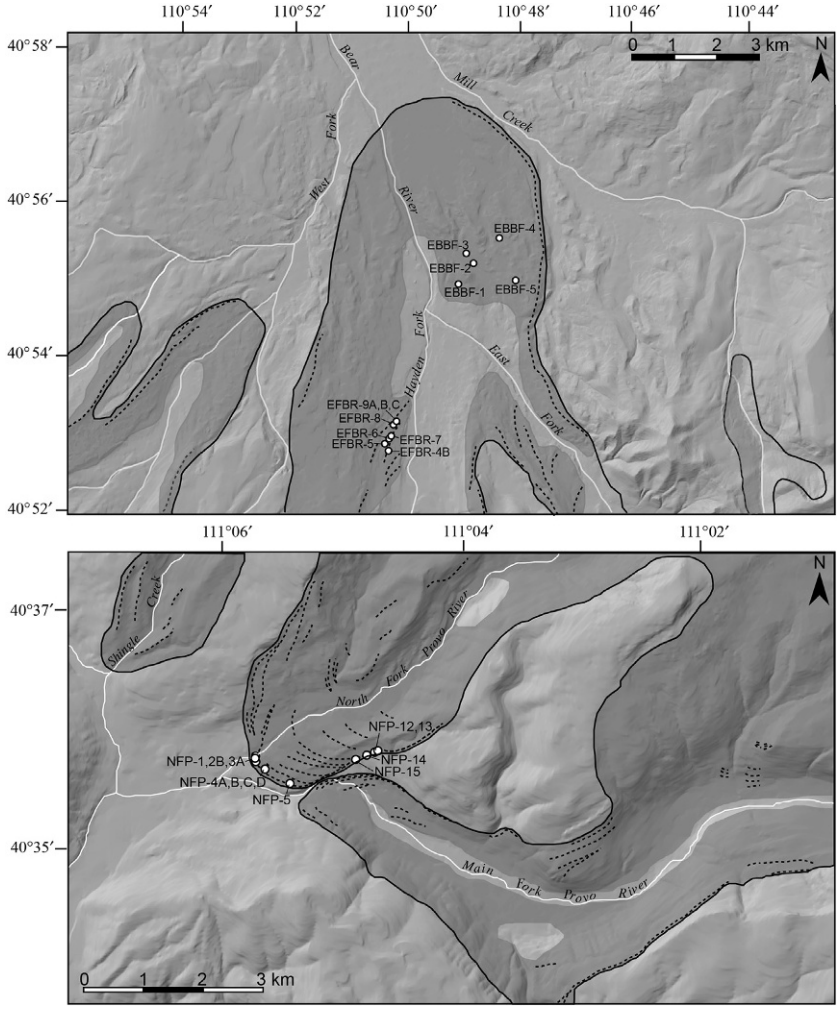

FIG. 17.6 Shaded-relief maps of the terminal moraine areas of the Bear River (top panel) and the Provo River (bottom panel) valleys. *Black lines* indicate the maximum ice extent. *Dashed lines* indicate moraine crests. *Darkened areas* indicate the extent of glacial till. Moraine boulder sample locations (*circles*) and *numbers* refer to samples shown in Table 17.2 and described in Laabs et al. (2009).

Weber, and Bear Rivers (Fig. 17.6), the latter being the largest river (in terms of drainage area) entering Lake Bonneville. In these and other valleys of the Uinta Mountains, glacial deposits are more widespread than in the Wasatch Mountains, due to a lesser degree of postglacial modification and generally larger glaciers. In all three valleys, moraines are well preserved, clearly .delimiting terminal ice positions during the last glaciation.

The Bear River valley was occupied by the largest sector of the Western Uinta Icefield and another, significantly smaller valley glacier. The icefield thickness exceeded 500 m in the largest troughs and formed an extensive piedmont lobe beyond the mountain front. A broad, high-relief, hummocky moraine that grades into an extensive outwash surface delimits the shape of the piedmont lobe. Up valley, recessional moraines are preserved in the East Fork and Hayden Fork of Bear River (Fig. 17.6a), indicating the terminal position of tributary glaciers during a stillstand or minor readvance of ice following construction of the piedmont moraine.

West of the Bear River valley, a smaller sector of the Western Uinta Icefield extended into the headwaters of the Weber River. Here, two large outlets of the Western Uinta Icefield occupied the Red Pine Creek tributary and the main valley of the Weber River, as indicated by well-preserved terminal moraines. A smaller outlet glacier terminated within a narrow canyon of the South Fork of Weber River (Fig. 17.5). Several small valley glaciers were present in high elevation tributary valleys of the Weber River, representing the westernmost extent of glaciation in the Uinta Mountains (Oviatt, 1994; Refsnider et al., 2007; Munroe and Laabs, 2009).

Across the westernmost summit of the Uinta Mountains are the headwaters of the Provo River, which featured the smallest sector of the Western Uinta Icefield (Refsnider et al., 2007). Most of this sector occupied the broad uplands at the heads of the North and South Forks of the Provo River, with smaller masses present in the Shingle, Coop, and Yellow Pine valleys (Munroe and Laabs, 2009). Detailed mapping by Refsnider et al. (2007) delimits the terminal position in the North Fork tributary during the last two glaciations, as well as the pattern of ice retreat up valley of the terminal moraine of the last glaciation. Glacial deposits are relatively sparse in the South Fork tributary, where only a few moraine segments are preserved above the confluence with the North Fork tributary and along Soapstone Creek. As a result, the up-valley extent of ice is less clear compared to other sectors of the western Uinta Icefield. The terminal position is clear, however, delimited by a set of small but well-preserved moraines near the terminal position in the North Fork tributary (Fig. 17.6).

Excellent preservation of glacial deposits throughout the Uinta Mountains, combined with 1:24,000-scale mapping in recent decades, afford reconstruction of glacier ELAs (Munroe et al., 2006). The sharp, west-to-east rise in glacier ELAs along the length of the Uinta Mountains (Fig. 17.3) has been interpreted to reflect a significant decline in precipitation along the range (Munroe and Mickelson, 2002; Munroe et al., 2006). This rise is too great to be explained by a west-to-east decline in precipitation due to simple orographic effects (Munroe and Mickelson, 2002; Laabs et al., 2006). Rather, the rise in ELAs may signify a declining impact of Lake Bonneville on glacier mass balance with distance away from the lake. This is further evidenced by

the formation of the large western Uinta Icefield at the west end of the range and smaller, discrete valley glaciers at the east end (Munroe, 2005).

In addition to the reconstruction of ELAs for glaciers throughout the Uinta Mountains (Munroe et al., 2006; Table 17.1), the volume of ice in the Western Uinta Icefield can be approximated by applying area–volume scaling models for valley glaciers at steady state (Bahr et al., 1997; Radić et al., 2007; Table 17.1). This method was applied to glacial valleys where the planimetric surface area of the ice is known from mapping-based reconstructions. Although ice extents are not precisely known for several glacial valleys in the Wasatch Mountains, it is known for the largest valley glaciers in the range (Fig. 17.4). Volume calculations indicate that ice volume was an order of magnitude greater in the Bear, Weber, and Provo River sectors of the Western Uinta Icefield than in the entire Wasatch Mountains (Table 17.1). Furthermore, the total ice volume in the Uinta and Wasatch segments of the LBB (247 km^3) was approximately 2.9% of the volume of Lake Bonneville (8603 km^3), as determined by computing the volume below 1552 m in the 30-m digital elevation model of the LBB shown in Fig. 17.1. The total volume of ice in all 13 other glaciated mountains of the LBB is incompletely known, but based on surface area alone (Fig. 17.1) it comprises less than 5% of the total ice volume in the Wasatch Mountains. The total volume of ice in the LBB was therefore less than 3.5% of the volume of the lake, representing a minor component of the lake water budget.

17.2.3 Central and Southern Utah

Several mountains and parts of the Colorado Plateau draining into the southeastern sector of the LBB were glaciated, including the Wasatch, Sevier, Markagunt and Fish Lake Plateaus, and the Pahvant and Tushar Ranges (Osborn and Bevis, 2001; Marchetti, 2007; Fig. 17.1). The glacial record in these areas is briefly summarized here. For a more-detailed description of glacial deposits in these settings and reconstructions of ice extent, the reader is referred to the useful review by Marchetti (2007) and references therein.

The most extensively glaciated areas of central Utah were the Wasatch Plateau (Foley et al., 1986; Larsen, 1996), Boulder Mountain (Marchetti et al., 2005), and Fish Lake Plateau (Marchetti et al., 2011). Among these, the greatest volume of ice formed on the Wasatch Plateau just outside of the LBB divide, where east-flowing drainages display well-developed cirques and broad U-shaped valleys eroded into Cenozoic sedimentary rocks (Larsen, 1996). Moraines of the last glaciation are identified by their preservation and minimal weathering characteristics (Osborn and Bevis, 2001), delimiting terminal positions in most glacial valleys, and affording accurate reconstructions of ice extent. Fish Lake Plateau is a faulted upland composed of Tertiary volcanics that featured a small ice cap during the last glaciation (Marchetti, 2007;

Marchetti et al., 2011). Multiple moraine sets deposited by small cirque glaciers likely record ice advance during multiple Pleistocene glaciations (DeGraff and Gallegos, 1983). Moraines of the last glaciation include large boulders suitable for cosmogenic ^{3}He exposure dating, providing a key chronology of the last glaciation in central Utah (Marchetti et al., 2011). Age limits on the last glaciation from Fish Lake Plateau and from the nearby Boulder Mountain (Marchetti et al., 2005) are described later.

The largest glaciers outside of the Wasatch and Fish Lake Plateaus occupied two valleys draining the Markagunt Plateau (Mulvey et al., 1984; Osborn and Bevis, 2001). The glacier occupying Castle Creek attained a length of approximately 5 km, as delimited by a hummocky terminal moraine. More extensive ice in the vicinity of the summit of the Markagunt Plateau (Brian Head) is also possible, although glacial deposits and landforms are poorly preserved (if present at all) outside the Castle and Lowder Creek valleys (Osborn and Bevis, 2001).

The glacial record of the Sevier Plateau, the Pahvant Range, and the Tushar Mountains includes deposits of the last glaciation recognized in previous mapping in central Utah (summarized by Osborn and Bevis, 2001; Marchetti, 2007). Although glacial features are preserved in each of these settings, glacier ice was sparse and moraines are assigned to the last glaciation solely on the basis of preservation and surface weathering characteristics (eg, Bevis, 1995).

Marchetti (2007) summarized glacier ELAs for the Tushar and Pahvant Ranges and the Wasatch Plateau as estimated in previous studies. These range from approximately 2800 m asl in the Wasatch Plateau and Pahvant Range to nearly 3300 m asl in the Tushar Range (Marchetti, 2007 and references therein). The greater ELAs relative to the Wasatch Mountains and the mean ELA in the Uinta Mountains may be attributed to the lower latitude of glaciers in these settings, but may also reflect a stronger orographic effect in the Wasatch Mountains resulting in greater precipitation. Marchetti (2007) also attributes the variability of ELAs in central Utah to redistribution of snow by wind, such that wind-deposited snow Wasatch Plateau and Pahvant Range may have enhanced glacier mass balance and locally depressed the ELA.

17.2.4 Western Ranges

The western border of the LBB, consisting of generally smaller and fragmented mountains of the Basin and Range relative to the east, was sparsely glaciated. The South and North Snake Ranges and the Deep Creek Range featured small cirque and valley glaciers during the last glaciation (Osborn and Bevis, 2001). Glacial deposits in all three ranges were mapped by Bevis (1995) and subdivided based on weathering characteristics.

Among these three ranges, cirque and valley glaciers were most numerous in the South Snake Range, a rare setting where summit elevations in the Basin and

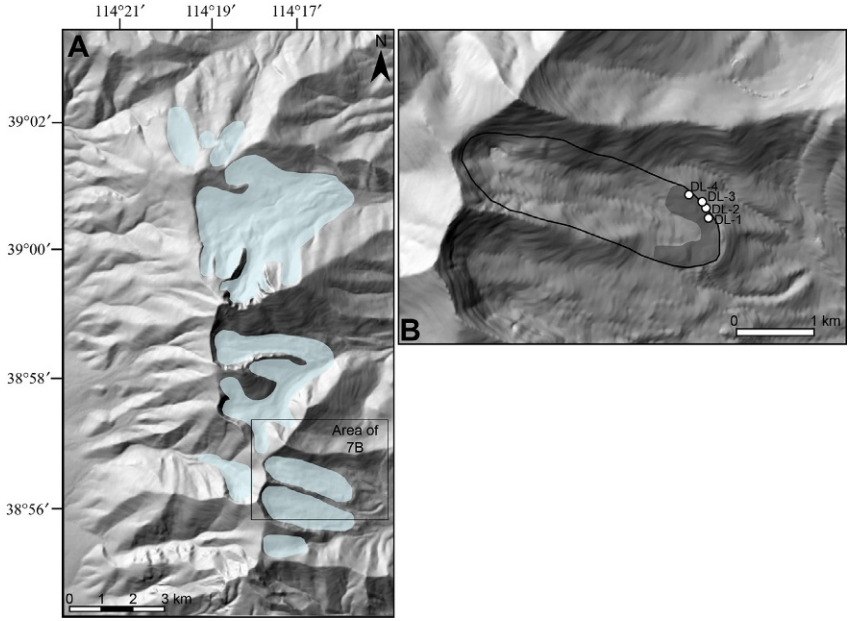

FIG. 17.7 Shaded-relief maps of (a) the glaciated portion of the South Snake Range, Nevada and (b) the northern tributary of the Snake Creek valley (produced from a mosaic of 10-m digital elevation models from http://epa.gov). Pleistocene ice extents are transparent *light blue* in (a) and outlined in *black* in (b). Darkened area in (b) is the terminal moraine. Moraine boulder sample locations (*circles*) and *numbers* refer to samples shown in Table 17.2.

Range exceed 4000 m asl (Fig. 17.7). At least 10 glacial valleys are identified in this range, each displaying well-developed cirques and U-shaped valleys noted in the early surveys of the Basin and Range (eg, Russell, 1885). Terminal moraines are preserved in some but not all glacial valleys. Piegat (1980) assigned moraines in several valleys to the Lamoille (penultimate) and Angel Lake (last) Glaciations, following terminology for Pleistocene glaciations in the Great Basin coined by Sharp (1938). The best-preserved moraine of the last glaciation is in the Snake Creek valley, forming a wide, hummocky moraine plateau in the vicinity of Dead Lake. This moraine features large boulders at the crest suitable for cosmogenic ^{10}Be exposure dating. Exposure ages of the moraine are given later. The largest valley glaciers in the South Snake Range occupied the Lehman and Baker Creek valleys, attaining maximum lengths of nearly 6 km (Osborn and Bevis, 2001).

The North Snake Range features four glacial valleys in the vicinity of the highest peak, Mt. Moriah (Piegat, 1980). Osborn and Bevis (2001) noted that a moraine deposited by a small cirque glacier displays surficial characteristics similar to that of moraines of the last glaciation elsewhere in the Great Basin. Piegat (1980) did not assign glacial deposits in the North Snake Range to a

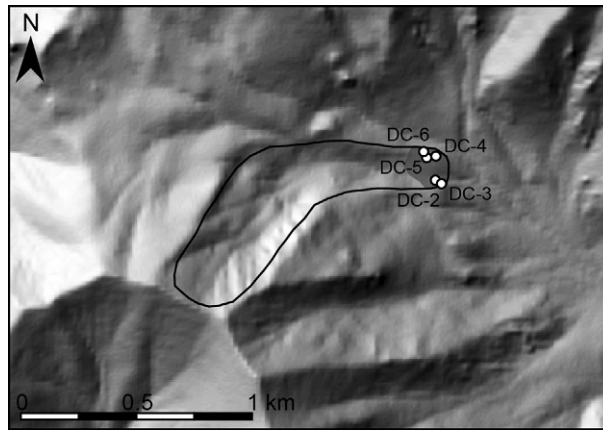

FIG. 17.8 Shaded-relief map of a portion of the Ibapah Peak, Deep Creek Mountains, digital elevation model (from http://epa.gov). Ice extent in a tributary of Granite Creek is outlined in *black*. *Darkened area* is the terminal moraine. Moraine boulder sample locations (*circles*) and *numbers* refer to samples shown in Table 17.2.

specific glaciation. Sparse preservation of moraines precludes an accurate reconstruction of ice extent and meaningful estimates of glacier ELAs.

Glacial deposits in the Deep Creek range, a remote range in western Utah more than 140 km north of the Snake Ranges, were identified by Bevis (1995) and Osborn and Bevis (2001). Bevis (1995) mapped moraines in four valleys and assigned terminal moraines to the last two Pleistocene glaciations based on preservation and weathering characteristics. A moraine in Granite Creek features large boulders suitable for cosmogenic ^{10}Be exposure dating (Fig. 17.8). Exposure ages of this moraine are given later.

At 2800–3000 m asl, ELAs of the South Snake and Deep Creek Ranges are similar to one another and to those reported for the central Utah ranges and plateaus, despite being on opposite sides of Lake Bonneville. This similarity suggests that Lake Bonneville did not enhance glacier mass balance in the central Utah ranges, other than possible local effects in the Wasatch Plateau and Pahvant Range.

17.2.5 Northern Ranges

Three small ranges in the north-central sector of the LBB, the Raft River, Stansbury and Oquirrh Ranges (Fig. 17.1), featured minor ice masses during the last glaciation. Glaciers in the Stansbury and Oquirrh Ranges were completely within the LBB. In contrast, only one small glacier in the Raft River Range flowed into Lake Bonneville, whereas other small ice masses in the range flowed northward and ultimately drained into the Snake River (Osborn and Bevis, 2001).

Glacial valleys appear in the northern segments of the Stansbury and Oquirrh Ranges, which were nearly surrounded by Lake Bonneville. These valleys are easily identified by well-developed cirques and U-shaped valleys in the Stansbury Range. Terminal and lateral moraines of the last glaciation are preserved in most valleys, indicating a maximum glacier length of 2.5–3 km in some east-flowing valleys (Osborn and Bevis, 2001). Conversely, glacial valleys are more difficult to identify in the Oquirrh Range due to weaker preservation of glacial erosional landforms and limited preservation of moraines. Here, glaciers were smaller in length and in number compared to the Stansbury Range (Osborn and Bevis, 2001).

In both ranges, glacial features are preserved well enough to enable reconstruction of ice extent and ELA in some valleys. ELAs in the two mountains follow the west-to-east decline across the northern sector of Lake Bonneville, displaying altitudes between those to the west and the Wasatch Mountains to the east (Table 17.1; Fig. 17.3).

17.3 CHRONOLOGY OF THE LAST GLACIATION

As described earlier, stratigraphic relationships between glacial and lacustrine deposits are limited to the western Wasatch Mountains, yet even there, previous stratigraphic models from the same glacial valley support different conclusions (Scott, 1988; Godsey et al., 2005). The lack of a complete stratigraphic record, combined with the limited number of numerical age limits on glacial deposits in the LBB, has for decades precluded a definitive understanding of the relative timing of glacier advance and retreat relative to the rise and fall of Lake Bonneville. This section presents chronologies of moraines in the basin based on cosmogenic ^{10}Be exposure dating of erratic boulders atop moraine crests. Most of the ages reported here are recalculated from previous work by the authors and their colleagues in the Wasatch and western Uinta Mountains (eg, Munroe et al., 2006; Laabs et al., 2009; Laabs et al., 2011). In addition, new cosmogenic ^{10}Be exposure ages from the western Wasatch, South Snake and Deep Creek Ranges are presented. The cosmogenic ^{3}He chronologies of glacial deposits in central Utah (Marchetti et al., 2005; Marchetti et al., 2011) are discussed later for comparison but are not recalculated. All of the available cosmogenic chronologies of terminal and recessional moraines are compared to the timing of high lake events in the LBB as described by Oviatt (2015).

Field and laboratory protocols involved in cosmogenic ^{10}Be exposure dating of moraine boulders in the Wasatch and Uinta Mountains are described in the original reports by Refsnider et al. (2008) and Laabs et al. (2009, 2011). Field and laboratory methods involved in cosmogenic ^{10}Be exposure dating of moraines in the western Wasatch, South Snake, and Deep Creek Ranges follow those of Laabs et al. (2013). Measurements of ^{10}Be/^{9}Be by accelerator mass spectrometry were done at the Purdue Rare Isotope Measurement Laboratory (PRIME Lab; Muzikar et al., 2003).

17.3.1 Calculations of Cosmogenic ^{10}Be Exposure Ages

Two recent reports of cosmogenic ^{10}Be exposure ages of moraines in the Wasatch and Uinta Mountains (Laabs et al., 2009, 2011) computed ages using a globally averaged, spallogenic-production rate, scaled for latitude and altitude using a model that assumes time-constant production of ^{10}Be (Balco et al., 2008). Since these reports were published, numerous additional calibrations of the spallogenic production of ^{10}Be have become available (as summarized by Borchers et al., 2016), nearly all of which yield a more precise and significantly lower reference production rate. Until recently, however, no surfaces with independent numerical ages were targeted for calibration of the ^{10}Be production rate in the western United States. That changed when Lifton et al. (2015, 2016) reported a calibrated ^{10}Be production rate model based on measurement of ^{10}Be concentrations in samples of two well-dated surfaces of Lake Bonneville deposits at Promontory Point in northern Utah. This model is useful for calculating the ^{10}Be production rate of late Pleistocene moraines in the LBB because of: (1) their proximity of the calibration site; and (2) the fact that the moraines and the surface used for the calibration both formed during the last glaciation.

In addition to this new, locally calibrated, production rate model, a separate study by Lifton et al. (2014) provides a new, physically based model for scaling the production of in situ ^{10}Be for latitude, altitude, and time. This model, termed the "LSD" (Lifton-Sato-Dunai) scaling scheme by Lifton et al. (2014), represents the most recent and robust consideration of the effects of geomagnitude latitude, atmospheric depth, and time on the spallogenic and muonic production of ^{10}Be. As discussed by Phillips et al. (2016), this model has the advantage of a stronger physical basis for computing the production of ^{10}Be and performs among the best of all available scaling models in a statistical analysis of known and predicted ages of calibration sites worldwide (Borchers et al., 2016). Given these advantages, and the risks of relying on a single calibration site, previously published and new cosmogenic ^{10}Be exposure ages reported here are recalculated using scaling factors generated by the LSD scaling model (Lifton et al., 2014) and a reference production rate of 4.0 ± 0.1 atoms g^{-1} $year^{-1}$ (after Shakun et al., 2015). As shown in the following paragraphs and Table 17.2, cosmogenic ^{10}Be exposure ages of moraines computed using the locally calibrated production model from Promontory Point and the LSD scaling factors yielded statistically overlapping exposure ages with central tendencies (mean and error-weighted mean ages) that differ by only hundreds of years. For consistency with Lifton et al. (2016), description of cosmogenic ^{10}Be exposure ages hereafter refers only to ages computed by the LSD scaling model. Recalculating cosmogenic ^{10}Be exposure ages in this way does not affect the distribution of ages about the central tendency. Rather, individual ages are uniformly ~10% older than initially reported and maintain their distribution. Because exposure ages from all but one moraine discussed later (the left-lateral segment of the moraine at

TABLE 17.2 ^{10}Be Data and Surface Exposure Ages for Moraines in the Lake Bonneville Basin

Moraine and Sample ID	Latitude (°N)	Longitude (°W)	Elevation (m asl)	Sample Thickness (cm)	Topographic Shielding Factor	Erosion Rate (cm/year)[a]	[^{10}Be] (Atoms g SiO_2^{-1})[b]	1σ	LSD Spall. Scaling Factor[c]	LSD Muon Scaling Factor[c]	LSD Exposure Age (ka)[d]	1σ External (kyr)[e]	Promontory Point-Lm Exposure Age (ka)[f]	1σ External (kyr)[e]
Wasatch—Little Cottonwood Canyon terminal														
02-UT-LCC-01	40.5823	−111.7973	1584	3	0.998	0.0003	2.54×10^5	8.21×10^3	3.282	1.409	**18.8**	**0.9**	**17.6**	**0.9**
02-UT-LCC-02	40.5815	−111.7938	1612	1.8	0.997	0.0003	2.46×10^5	6.53×10^3	3.343	1.417	**17.6**	**0.7**	**16.6**	**0.8**
02-UT-LCC-04	40.5828	−111.7937	1601	2	0.997	0.0003	2.48×10^5	6.32×10^3	3.317	1.414	**18.0**	**0.7**	**16.9**	**0.8**
02-UT-LCC-05	40.5828	−111.7934	1605	3	0.997	0.0003	2.61×10^5	6.56×10^3	3.337	1.415	**19.0**	**0.8**	**17.8**	**0.8**
02-UT-LCC-06	40.5817	−111.7948	1605	2	0.998	0.0003	2.44×10^5	6.13×10^3	3.325	1.415	**17.6**	**0.7**	**16.5**	**0.8**
02-UT-LCC-07	40.5823	−111.7931	1605	2	0.997	0.0003	2.43×10^5	6.22×10^3	3.325	1.415	**17.6**	**0.7**	**16.5**	**0.8**
02-UT-LCC-08	40.5808	−111.7935	1611	2	0.997	0.0003	2.70×10^5	7.04×10^3	3.357	1.417	**19.4**	**0.8**	**18.2**	**0.9**
										Mean (n=7, χ^2R=1.02[g], 1σ) = **18.3 ± 0.8**		Mean (n=7, χ^2R=0.69, 1σ) = **17.2 ± 0.7**		
Wasatch—Little Cottonwood Canyon lateral														
LCL-1	40.5705	−111.7941	1695	3	0.995	0.0003	1.98×10^5	6.74×10^3	3.534	1.443	**14.7**	**0.7**	**14.0**	**0.7**
LCL-2	40.5701	−111.7917	1714	1.5	0.992	0.0003	2.61×10^5	1.11×10^4	3.631	1.450	**18.9**	**1.1**	**18.1**	**1.1**
LCL-4	40.5704	−111.7938	1711	6	0.992	0.0003	4.07×10^5	1.92×10^4	3.748	1.451	**27.4**	**1.7**	**26.8**	**1.7**
LCL-5B	40.5702	−111.7919	1709	4	0.992	0.0003	1.62×10^5	5.58×10^3	3.559	1.446	**12.0**	**0.6**	**11.4**	**0.6**
LCL-6	40.5702	−111.7922	1706	2.5	0.995	0.0003	2.29×10^5	1.10×10^4	3.588	1.447	**16.7**	**1.0**	**16.1**	**1.0**
LCL-7	40.5702	−111.7925	1704	3.5	0.995	0.0003	3.21×10^5	1.47×10^4	3.685	1.448	**23.5**	**1.4**	**22.9**	**1.4**
LCL-9	40.5703	−111.7927	1699	2.5	0.996	0.0003	2.18×10^5	1.09×10^4	3.563	1.445	**16.0**	**1.0**	**15.3**	**1.0**
										Mean (n=7, χ^2R=32.43, 1σ) = **18.5 ± 5.3**		Mean (n=7, χ^2R=32.29, 1σ) = **17.8 ± 5.3**		

Continued

TABLE 17.2 ^{10}Be Data and Surface Exposure Ages for Moraines in the Lake Bonneville Basin—Cont'd

Moraine and Sample ID	Latitude (°N)	Longitude (°W)	Elevation (m asl)	Sample Thickness (cm)	Topographic Shielding Factor	Erosion Rate (cm/year)	[^{10}Be] (Atoms g SiO_2^{-1})	1σ	LSD Spall. Scaling Factor	LSD Muon Scaling Factor	LSD Exposure Age (ka)	1σ External (kyr)	Promontory Point-Lm Exposure Age (ka)	1σ External (kyr)
Wasatch—American Fork terminal														
AF-1	40.5200	−111.6197	2296	6	0.986	0	3.95×10^5	1.44×10^4	5.542	1.651	**17.2**	**0.8**	**16.6**	**0.9**
AF-2	40.5184	−111.6208	2312	3	0.994	0	3.91×10^5	1.69×10^4	5.596	1.656	**16.4**	**0.9**	**15.8**	**0.9**
AF-3	40.5177	−111.6208	2313	4	0.995	0	4.75×10^5	1.90×10^4	5.666	1.658	**19.7**	**1.0**	**19.2**	**1.0**
AF-4	40.5179	−111.6212	2312	2.5	0.993	0	4.53×10^5	1.23×10^4	5.634	1.657	**18.7**	**0.8**	**18.2**	**0.8**
AF-6	40.5193	−111.6206	2318	4	0.992	0	3.90×10^5	3.04×10^4	5.620	1.658	**16.4**	**1.4**	**15.9**	**1.4**
AF-7	40.5160	−111.6234	2285	4	0.992	0	3.38×10^5	1.52×10^4	5.453	1.645	**14.7**	**0.8**	**14.1**	**0.8**
AF-8	40.5168	−111.6236	2295	4.5	0.995	0	4.73×10^5	1.78×10^4	5.601	1.652	**19.9**	**1.0**	**19.4**	**1.0**
AF-9	40.5158	−111.6236	2283	4	0.994	0	3.92×10^5	1.13×10^4	5.486	1.646	**16.9**	**0.7**	**16.3**	**0.8**
AF-10	40.5185	−111.6223	2311	4.5	0.990	0	4.01×10^5	1.74×10^4	5.598	1.656	**17.0**	**0.9**	**16.5**	**0.9**
AF-11	40.5185	−111.6223	2311	4	0.990	0	3.93×10^5	7.97×10^3	5.595	1.656	**16.6**	**0.6**	**16.1**	**0.7**
										Mean (n=10, χ^2R=3.29, 1σ) =**17.4±1.6**		Mean (n=10, χ^2R=3.36, 1σ) =**16.8±1.6**	
Wasatch—Bells Canyon lateral														
BCR-1	40.56673	−111.78936	1803	4	0.9861	0	3.12×10^5	1.22×10^4	3.922	1.480	**20.6**	**0.8**	**20.0**	**0.8**
BCR-2	40.56674	−111.78958	1804	4	0.9859	0	3.81×10^5	1.31×10^4	3.990	1.482	**24.7**	**0.9**	**24.5**	**0.9**
BCR-4	40.56687	−111.79041	1800	4	0.9919	0	3.56×10^5	1.03×10^4	3.962	1.480	**23.1**	**0.8**	**22.8**	**0.8**
										Mean (n=3, χ^2R=6.08, 1σ) =**22.8±2.1**		Mean (n=3, χ^2R=7.37, 1σ) =**22.4±2.3**	

Wasatch—Bells Canyon recessional														
BCLR-1	40.56338	−111.79162	1741	4	0.987	0	2.42×10^5	9.07×10^3	3.6857	1.4585	**16.9**	**0.6**	**16.2**	**0.6**
BCLR-2	40.56338	−111.79162	1741	4	0.9889	0	2.58×10^5	7.62×10^3	3.6953	1.4588	**17.9**	**0.6**	**17.2**	**0.6**
										Mean (n=2, χ^2R=1.39, 1σ) =**17.4 ± 0.7**		Mean (n=2, χ^2R=1.39, 1σ) =**16.7 ± 0.7**		
Uinta—Bear River terminal														
EBBF-1	40.9178	−110.8210	2646	4.5	1	0	5.48×10^5	3.00×10^4	7.199	1.790	**17.7**	**1.2**	**17.7**	**1.2**
EBBF-2	40.9224	−110.8210	2593	6.5	1	0	5.83×10^5	2.86×10^4	7.017	1.770	**19.6**	**1.2**	**19.8**	**1.2**
EBBF-3	40.9241	−110.8210	2592	6.5	1	0	5.34×10^5	1.48×10^4	6.948	1.768	**18.2**	**0.8**	**18.2**	**0.8**
EBBF-4	40.9280	−110.8210	2578	3.5	1	0	5.70×10^5	3.11×10^4	6.915	1.764	**19.0**	**1.3**	**19.1**	**1.3**
EBBF-5	40.9181	−110.8210	2645	4.5	1	0	6.24×10^5	3.73×10^4	7.287	1.792	**19.9**	**1.4**	**20.1**	**1.4**
										Mean (n=5, χ^2R=0.65, 1σ) =**18.9 ± 0.9**		Mean (n=5, χ^2R=0.80, 1σ) =**19.0 ± 1.0**		
Uinta—Bear River lateral														
EFBR-1	40.8799	−110.7947	2757	4	1	0	5.18×10^5	5.09×10^4	7.711	1.834	**15.6**	**1.6**	**15.7**	**1.6**
EFBR-4A	40.8788	−110.8417	2640	4.5	1	0	7.29×10^5	1.34×10^5	7.355	1.792	**23.1**	**4.4**	**23.5**	**4.4**
EFBR-4B	40.8788	−110.8417	2640	4	1	0	6.46×10^5	2.47×10^4	7.286	1.790	**20.6**	**1.1**	**20.8**	**1.1**
EFBR-5	40.8805	−110.8429	2651	5	1	0	6.44×10^5	2.85×10^4	7.342	1.795	**20.5**	**1.2**	**20.8**	**1.2**
EFBR-7	40.8822	−110.8409	2646	3	1	0	6.41×10^5	5.97×10^4	7.298	1.792	**20.2**	**2.1**	**20.4**	**2.1**
EFBR-8	40.8847	−110.8403	2640	4.5	1	0	6.45×10^5	2.28×10^4	7.292	1.790	**20.6**	**1.1**	**20.9**	**1.1**
EFBR-9A	40.8855	−110.8394	2654	5	1	0	5.92×10^5	2.60×10^4	7.275	1.794	**19.0**	**1.1**	**19.1**	**1.1**
EFBR-9B	40.8855	−110.8394	2654	4.5	1	0	7.13×10^5	4.06×10^4	7.415	1.797	**22.4**	**1.6**	**22.8**	**1.6**
EFBR-9C	40.8855	−110.8394	2654	5	1	0	5.76×10^5	2.62×10^4	7.255	1.793	**18.5**	**1.1**	**18.6**	**1.1**
										Mean (n=9, χ^2R=1.74, 1σ) =**20.1 ± 2.2**		Mean (n=9, χ^2R=1.93, 1σ) =**20.3 ± 2.3**		

Continued

TABLE 17.2 ^{10}Be Data and Surface Exposure Ages for Moraines in the Lake Bonneville Basin—Cont'd

Moraine and Sample ID	Latitude (°N)	Longitude (°W)	Elevation (m asl)	Sample Thickness (cm)	Topographic Shielding Factor	Erosion Rate (cm/year)	[^{10}Be] (Atoms g SiO_2^{-1})	1σ	LSD Spall. Scaling Factor	LSD Muon Scaling Factor	LSD Exposure Age (ka)	1σ External (kyr)	Promontory Point-Lm Exposure Age (ka)	1σ External (kyr)
Uinta—North Fork Provo terminal														
NFP-1	40.5985	−111.0942	2319	5	1	0	3.22×10^5	1.56×10^4	5.597	1.659	**13.4**	**0.8**	**13.1**	**0.8**
NFP-2B	40.7023	−111.0945	2327	3	1	0	4.35×10^5	1.53×10^4	5.714	1.664	**17.5**	**0.9**	**17.2**	**0.9**
NFP-3A	40.7020	−111.0937	2321	6	1	0	4.81×10^5	5.16×10^4	5.747	1.663	**19.7**	**2.2**	**19.5**	**2.2**
NFP-4A	40.5965	−111.0927	2324	5	0.999	0	4.73×10^5	1.32×10^4	5.723	1.663	**19.3**	**0.9**	**19.0**	**0.9**
NFP-4B	40.5963	−111.0927	2324	2.5	1	0	3.91×10^5	1.94×10^4	5.659	1.661	**15.8**	**1.0**	**15.5**	**1.0**
NFP-4C	40.5963	−111.0927	2324	3	1	0	3.75×10^5	1.86×10^4	5.645	1.661	**15.2**	**0.9**	**15.0**	**0.9**
NFP-4D	40.5963	−111.0927	2324	3	0.999	0	5.33×10^5	2.55×10^4	5.798	1.665	**21.1**	**1.3**	**21.0**	**1.3**
NFP-5	40.5946	−111.0870	2346	3.5	1	0	4.39×10^5	1.18×10^4	5.771	1.670	**17.5**	**0.8**	**17.2**	**0.8**
										Mean (n=8, χ^2R=6.80, 1σ) =**17.4 ± 2.6**		Mean (n=8, χ^2R=6.95, 1σ) =**17.2 ± 2.6**		
Uinta—North Fork Provo lateral														
NFP-12	40.6006	−111.0719	2505	6	1	0	4.93×10^5	1.50×10^4	6.465	1.731	**17.9**	**0.9**	**17.8**	**0.9**
NFP-13	40.6007	−111.0718	2504	4.5	1	0	5.11×10^5	1.52×10^4	6.470	1.731	**18.4**	**0.9**	**18.2**	**0.9**
NFP-14	40.6003	−111.0733	2489	3	0.999	0	5.42×10^5	1.49×10^4	6.435	1.726	**19.4**	**0.9**	**19.3**	**0.9**
NFP-15	40.5996	−111.0753	2471	2.5	0.999	0	5.37×10^5	1.80×10^4	6.355	1.719	**19.3**	**1.0**	**19.2**	**1.0**
										Mean (n=4, χ^2R=0.62, 1σ) =**18.8 ± 0.7**		Mean (n=4, χ^2R=0.65, 1σ) =**18.6 ± 0.7**		

Deep Creek—Granite Creek terminal														
DC-02	39.8062	−113.9146	2661	6	0.982	0	3.22×10^5	1.29×10^4	6.881	1.783	*12.4*	*0.7*	*12.2*	*0.7*
DC-05	39.8081	−113.9160	2678	4.5	0.979	0	5.30×10^5	1.93×10^4	7.130	1.794	**19.5**	**1.0**	**19.4**	**1.0**
DC-06	39.8079	−113.9159	2675	6	0.979	0	5.33×10^5	2.00×10^4	7.137	1.794	**19.9**	**1.0**	**19.8**	**1.0**
DC-03	39.8064	−113.9150	2666	3	0.978	0	5.52×10^5	2.02×10^4	7.111	1.790	**20.2**	**1.0**	**20.1**	**1.0**
DC-04	39.8079	−113.9152	2668	5	0.977	0	8.88×10^5	1.45×10^5	7.433	1.800	*31.7*	*5.4*	*32.1*	*5.4*
											Mean (n=3, χ^2R=0.12, 1σ) =**19.9 ± 0.4**		Mean (n=3, χ^2R=0.12, 1σ) =**19.8 ± 0.4**	
South Snake Range—Dead Lake terminal														
DL-1	38.9355	−114.2724	2912	2.5	0.997	0	5.47×10^5	2.34×10^4	7.976	1.881	**17.4**	**1.0**	**17.2**	**1.0**
DL-2	38.9361	−114.2724	2911	3	0.997	0	6.30×10^5	2.17×10^4	8.097	1.884	**19.9**	**1.0**	**19.8**	**1.0**
DL-4	38.9364	−114.2731	2912	4.5	0.995	0	5.19×10^5	2.18×10^4	7.959	1.881	**16.9**	**0.9**	**16.6**	**0.9**
DL-6	38.9367	−114.2734	2908	2.5	0.995	0	4.37×10^5	1.75×10^4	7.855	1.877	*14.1*	*0.8*	*13.9*	*0.8*
											Mean (n=3, χ^2R=2.74, 1σ) =**18.1 ± 1.6**		Mean (n=3, χ^2R=3.08, 1σ) =**17.9 ± 1.7**	

Notes: All samples have a density of 2.65 g/cm^3. All ^{10}Be measurements were completed by accelerator mass spectrometer (AMS) at PRIME Lab (Purdue University). All samples were measured against AMS standard coded as "KNSTD" in the CRONUS Earth online exposure age calculator, except for the LCL (other than LCL-4), DC and DL samples, which were measured against Beryllium AMS standard Be-01-5-3 (Nishiizumi et al., 2007), which is coded "07KNSTD" in the CRONUS Earth exposure age calculator.
Ages and uncertainties are indicated in bold. Discarded ages are italicized.
[a] *See Laabs et al. (2011) for explanation of inferred erosion rates of moraine boulders in the Wasatch Mountains.*
[b] *Blank-corrected concentration.*
[c] *Computed from the scaling model of Lifton et al. (2014).* LSD, *Lifton-Sato-Dunai.*
[d] *Computed from the LSD scaling factors given in two preceding columns.*
[e] *Uncertainty of AMS measurement and production rate.*
[f] *Computed from the calibrated production rate at Promontory Point (Lifton et al., 2015) with "Lm" scaling by the CRONUS online exposure age calculator, version 2.2 (Balco et al., 2008).*
[g] *For all moraines, this value is computed from the surface exposure ages ± the internal uncertainty.*

Little Cottonwood Canyon) are approximately normally distributed, we consider the mean age ($\pm 1\sigma$) to best represent the true age of the moraine. Competing effects of burial and prior exposure of erratic boulders may therefore cancel out in cases where the $\chi^2 R$ statistic is greater than one, indicating that observed scatter exceeds that predicted by analytical uncertainty (Balco et al., 2009).

17.3.2 Cosmogenic ^{10}Be Chronologies of Moraines in the Western Uinta and Wasatch Mountains

Cosmogenic ^{10}Be exposure ages in the western Wasatch Mountains are from three moraine segments in two glacial valleys, Little Cottonwood and American Fork Canyons (Fig. 17.4). The two dated segments of the moraine at the mouth of Little Cottonwood, the right latero-frontal segment and the left-lateral segment, yield overlapping mean ages ($\pm 1\sigma$) of 18.3 ± 0.8 and 18.5 ± 5.3 ka, respectively. The geological or analytical reasons for the unusually broad scatter among exposure dates from the left-lateral segment (Table 17.2) are unclear. Cosmogenic ^{10}Be exposure ages of the terminal moraine in American Fork Canyon overlap with these ages, with a mean of 17.4 ± 1.6 ka. Together, ^{10}Be exposure ages from the western Wasatch Mountains indicate that overall retreat from these moraines was nearly synchronous.

Five new cosmogenic ^{10}Be exposure ages of moraines in Bells Canyon provide some useful insight to whether ice occupied the western front of the Wasatch Mountains during the Last Glacial Maximum, which was unclear from the original report of Laabs et al. (2011). Samples were collected from three erratic boulders atop the right-lateral sector of the terminal moraine and two from a recessional moraine less than 500 m upvalley. Both moraines represent times when ice occupied the western front of the Wasatch Mountains. Three cosmogenic ^{10}Be exposure dates from the right-lateral sector of the terminal moraine and two from the recessional moraine yield mean ages of 22.8 ± 2.8 and 17.4 ± 0.7 ka, respectively. Together, these ages indicate that ice occupied the mountain front during portions of the transgressive and overflowing phases of Lake Bonneville. The mean cosmogenic ^{10}Be exposure age of the recessional moraine overlaps with those of the right-lateral sector of the terminal moraine at Little Cottonwood Canyon and the terminal moraine in American Fork Canyon, further supporting the observation that final deglaciation began after the Lake Bonneville highstand but during the overflowing phase.

The timing of glaciation in the western Uinta Mountains is indicated by cosmogenic ^{10}Be exposure ages of moraines in the Bear River and North Fork Provo valleys. The ice-proximal sector of the terminal moraine on the piedmont of the Bear River valley has a mean cosmogenic ^{10}Be exposure age of 18.9 ± 0.9 ka and a recessional lateral moraine in the East Fork of Bear River has a mean exposure age of 20.1 ± 2.2 ka. Because these moraines delimit the ice margin in a recessional position, their cosmogenic ^{10}Be exposure ages

represent minimum limits of the onset of overall ice retreat. Further limits on the start of ice retreat are available from radiocarbon ages of glacial flour identified in sediment cores of Bear Lake, downstream of the glaciated headwaters of the Bear River valley. These ages indicate a maximum in glacial-flour production at 20–19 ka, likely corresponding to the time of the glacier maximum or early ice retreat (Rosenbaum and Heil, 2009). Therefore, although the ^{10}Be exposure ages of the Bear River moraine segments overlap with those of moraines in the western Wasatch Mountains, the onset of ice retreat in Bear River likely occurred earlier.

In the North Fork Provo valley, cosmogenic ^{10}Be exposure ages of a terminal and left-lateral moraine indicate the onset of ice retreat at 17.4 ± 2.6 and 18.8 ± 0.7 ka, respectively. Overlapping ages between these two sectors of moraines are consistent with mapping of Refsnider et al. (2007), indicating that the two moraines are connected (Fig. 17.6). The possible reasons for the observed scatter among individual exposure ages from the terminal moraine are described in Refsnider et al. (2008). In any case, these exposure ages indicate that the onset of retreat of the North Fork Provo sector of the Western Uinta Icefield was in step with, or slightly later than, that of the Bear River sector and in step with the start of ice retreat in the western Wasatch Mountains.

17.3.3 Cosmogenic ^{10}Be Chronologies of Moraines in Western Ranges of the LBB

Cosmogenic ^{10}Be exposure ages of moraines in the western LBB are available from the Deep Creek and South Snake Ranges (Fig. 17.1; Table 17.2). In both settings, exposure ages of large erratic boulders atop a single-crested terminal moraine were determined, indicating the start of ice retreat in a single glacial valley (Table 17.2). In the South Snake Range, four cosmogenic ^{10}Be exposure ages have a mean age of 17.1 ± 2.4 ka, although the youngest of these does not overlap with the three oldest exposure ages within the measurement plus the production rate uncertainty (the latter is insignificant for comparing ages from the same moraine). Thus, the mean of the three oldest exposure ages, 18.1 ± 1.8 ka, provides a more accurate age of the moraine. In the Deep Creek Range, the oldest and youngest of five exposure ages do not overlap with any other ages in the population and are therefore considered outliers (Table 17.2). The mean of three overlapping exposure ages is 19.9 ± 0.4 ka. These ^{10}Be exposure ages are the first from the western LBB and are broadly consistent with those from the Wasatch and Uinta Mountains in the northeastern sector of the basin. Overall agreement among these ages (Fig. 17.9) suggests regional synchrony in the start of the last deglaciation.

17.3.4 The Pattern of the Last Glaciation in the LBB

Although chronological data are available for only a small number of glacial valleys in the LBB, the temporal pattern of the last glaciation provides a key

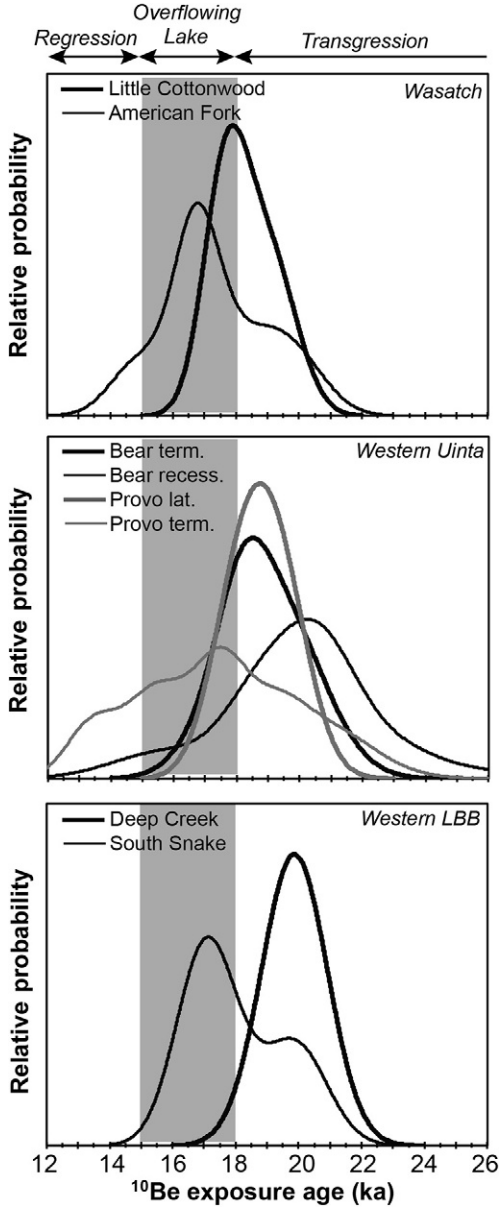

FIG. 17.9 Cumulative probably plots of cosmogenic ^{10}Be exposure ages of moraines in the Lake Bonneville basin relative to the transgressive (30–18 ka), overflowing (18–15 ka; *gray bar* on each plot), and regressive (15–12 ka) phases of Lake Bonneville, as defined by Oviatt (2015).

framework for understanding: (1) the relative timing of glaciation and the rise and fall of Lake Bonneville and (2) how climate changed during and after the last glaciation. The former is discussed here in light of the recalculated cosmogenic ^{10}Be exposure ages described earlier and additional age limits on glacial deposits in the LBB. The discussion is based on the chronology of Lake Bonneville as reviewed by Oviatt (2015), in which the transgressive (30–18 ka), overflowing (18–15 ka), and regressive (15–12.5 ka) phases of Lake Bonneville are identified largely on the basis of radiocarbon dating of shoreline deposits. This model reflects critical evaluation of a large number of radiocarbon dates and is broadly consistent with other recently reported chronologies of Lake Bonneville (eg, Benson et al., 2011; McGee et al., 2012; Miller et al., 2013).

The transgressive phase of Lake Bonneville began prior to, and ended after, the Last Glacial Maximum as defined by Clark et al. (2009) of 26.5–19.0 ka, a time when numerous mountain glaciers throughout the western United States attained their maximum extent (Shakun et al., 2015). In addition to cosmogenic ^{10}Be exposure ages of moraines in the western Uinta Mountains, Deep Creek and South Snake Ranges that fall within the latest part of the transgressive interval of the lake (Fig. 17.9), there is chronological and stratigraphic evidence indicating that glaciers in the western Wasatch Mountains attained their maxima prior to the overflowing phase of the lake. This includes stratigraphic observations of Scott et al. (1983) at the mouth of Little Cottonwood Canyon, where shoreline gravels of Lake Bonneville overlie weakly weathered till deposited during the last glaciation. Ice presence at the mountain front prior to the Lake Bonneville highstand is further evidenced by shoreline gravels overlying Pinedale age till comprising the distal slope of the moraine at Bells Canyon (Personius and Scott, 1992; Fig. 17.4).

Further support of glacier maxima during the transgressive phase of Lake Bonneville is yielded by cosmogenic ^{3}He exposure dating of moraines in central Utah (Marchetti et al., 2005, 2011). Terminal moraines of the last glaciation at Boulder Mountain (albeit just beyond the border of the LBB) and Fish Lake Plateau yield exposure ages corresponding to the Last Glacial Maximum, indicating that ice retreated from these moraines during the transgressive phase of Lake Bonneville.

Other terminal moraines in the LBB remained occupied, or were reoccupied, during the overflowing phase of the lake at 18–15 ka (Fig. 17.9). Cosmogenic ^{10}Be exposure ages of terminal moraines at Little Cottonwood and American Fork Canyons correspond to the time when Lake Bonneville overflowed, as does the mean age of the terminal moraine in the North Fork Provo River valley (Table 17.1; Fig. 17.9). The former ages are consistent with observations of interbedded till and lacustrine gravel near the mouth of Little Cottonwood Canyon of Godsey et al. (2005). East of the Provo River valley, a recessional moraine in the Uinta Mountains yields cosmogenic ^{10}Be exposure ages corresponding to the overflowing phase of Lake Bonneville, indicating

that, in at least one glacial valley (Lake Fork Canyon), a readvance or still-stand occurred at 18 ka (Laabs et al., 2009). A readvance during the overflowing phase of Lake Bonneville is also indicated by cosmogenic ^{3}He exposure ages of recessional moraines at Boulder Mountain (Marchetti et al., 2005).

A key revision of the glacial chronology from earlier reports is that even the youngest terminal moraines in the LBB were abandoned near, and possibly before, the time of the Bonneville flood at 18 ka (Oviatt, 2015). Based on earlier ^{10}Be production rate models, Laabs et al. (2009, 2011) described the significance of the apparent synchrony of terminal moraine abandonment and the onset of the regressive phase of Lake Bonneville. The recalculated ^{10}Be exposure ages reported here indicate that terminal moraines were abandoned in advance of the fall from the Provo shoreline at or after 15 ka (Miller et al., 2013, 2015).

What remains unchanged from earlier reports is the strong likelihood that glaciers in the LBB attained their maxima (possibly multiple times) during the transgressive phase of Lake Bonneville (Laabs et al., 2011) and the Last Glacial Maximum. This is consistent with the earliest models of the relative timing of glacier maxima and the Lake Bonneville highstand (Gilbert, 1890; Atwood, 1909), and considerations of the asymmetry of moraine volumes at the mouths of Little Cottonwood and Bells Canyons (Laabs et al., 2011). Additional stratigraphic observations of Lake Bonneville sediment and till at the mouths of Little Cottonwood and Bells Canyons may help to clarify: (1) whether tills buried by the shoreline gravels were deposited during the last glaciation instead of during an earlier glacial episode; and (2) the precise timing of the onset of glacier maxima.

17.4 INFERRED CLIMATE DURING THE LAST GLACIATION

17.4.1 Regional Records of Climate Change and Inferences from the Glacial Record

Based on the available stratigraphic observations and numerical age limits for glacial deposits, the glacial record throughout the LBB indicates that glacier maxima occurred prior to the highstand of Lake Bonneville (ie, $>$18 ka) and that overall ice retreat began prior to or during the period when the lake overflowed at 18–15 ka (Fig. 17.9) with some local readvances. Glacier maxima during the transgressive phase of Lake Bonneville and the Last Glacial Maximum were undoubtedly driven by global- and regional-scale cooling in response to insolation forcing and minimal greenhouse gas concentrations (Clark et al., 2009) and is consistent in time with age controls on mountain glacier maxima elsewhere in the western United States (Phillips et al., 2009; Laabs et al., 2013; Shakun et al., 2015).

The fact that glaciers attained their maxima while Lake Bonneville was below its highstand elevation provides clues to understanding the magnitude

of temperature and precipitation changes during the Last Glacial Maximum. Given that the length of mountain glaciers in continental interiors is largely controlled by temperature and radiation balance and that lakes are more sensitive to precipitation changes, climate in the LBB during the Last Glacial Maximum was likely cold and dry. This has been inferred in previous studies of glacial climate in the western United States (eg, Porter et al., 1983; Murray and Locke, 1989) and in the LBB (Kaufman, 2003), and is broadly consistent with atmosphere–ocean general circulation model simulations of the Last Glacial Maximum (eg, Bracconot et al., 2007). Amino-acid paleothermometry of Kaufman (2003) suggests that temperatures were 7–13°C colder than modern. Numerical modeling of the glacier in Little Cottonwood Canyon suggests that a temperature depression of 9°C or more was likely accompanied by less-than-modern precipitation (Laabs et al., 2006). A cold and drier-than-modern climate during the Last Glacial Maximum is consistent with the observation that Pleistocene lakes elsewhere in the Great Basin generally stood below their highstand elevations during the LGM (Munroe and Laabs, 2013), suggesting that precipitation levels were too low to sustain lakes at their highstands.

One possible interpretation of the correspondence of cosmogenic ^{10}Be exposure ages of some moraines and the start of the overflowing phase of Lake Bonneville (Fig. 17.9) is that climate in the LBB near the time of Bonneville highstand at 18 ka favored both glacier and lake maxima. If so, a cold and dry LGM climate may have transitioned into wetter conditions immediately post-LGM, favoring the expansion of lakes, and sustaining glaciers at or near their maxima. The retreat of the Laurentide Ice Sheet or hemisphere-scale effects of Heinrich Stadial 1 beginning after c.19 ka may have regionally affected atmospheric circulation in the western United States to permit the flow of southerly (Lyle et al., 2012) or westerly (Asmerom et al., 2010; Kirby et al., 2013; Oster et al., 2015), moisture-laden air into the Great Basin, regionally enhancing precipitation (Benson and Thompson, 1987; Licciardi et al., 2004; Thackray, 2008). Glacier modeling experiments and consideration of glacier ELAs in the northern LBB suggest that if temperature depression ranged from 6 to 9°C near the time of the Bonneville highstand, then precipitation was likely 1–2× modern (Laabs et al., 2006; Leonard, 2007; Refsnider et al., 2008) or possibly greater (Laabs et al., 2015). If greater precipitation sustained mountain glaciers in the LBB at their maxima at c.18 ka, then this effect may have been short lived as indicated by the onset of overall ice retreat at 18 ka or shortly thereafter (Fig. 17.9) while Lake Bonneville continued to overflow until c.15 ka and numerous lakes elsewhere in the Great Basin attained their maxima at c.17 ka (Munroe and Laabs, 2013). Cosmogenic ^{10}Be exposure ages of some moraines beyond the LBB indicate that glaciers in the Great Basin and northern Rocky Mountains persisted at or readvanced to their maximum extent until 17–16 ka (Licciardi et al., 2004; Laabs et al., 2013), suggesting that, at least locally, climate remained favorable for lake and glacier maxima after Lake Bonneville began to overflow.

Further development of the chronology of glacial deposits, especially recessional moraines, within and beyond the LBB will help to understand how climate changed during the overflowing phase of Lake Bonneville. In any case, glaciers within the LBB and elsewhere in the western United States were greatly diminished or absent during the regressive phase of Lake Bonneville. The onset of ice retreat prior to the regressive phase of the lake suggests that, despite the strong possibility of enhanced precipitation while Lake Bonneville overflowed, glacier mass balance declined prior to regional-scale warming of the Bølling–Allerød interval (Stanford et al., 2006). Retreat was likely in response to warming driven by rising summer insolation and atmospheric CO_2 (Shakun et al., 2015).

17.4.2 Hydrological and Climatic Effects of Lake Bonneville on Mountain Glaciers

The potential impact of Lake Bonneville on glaciers in neighboring mountains has been discussed in numerous previous reports (eg, Zielinski and McCoy, 1987; Hostetler et al., 1994; Munroe and Mickelson, 2002; Munroe et al., 2006; Laabs et al., 2011). In light of the ^{10}Be exposure ages reported here and other chronological data pertaining to the relative timing of glacier maxima and the overflowing phase of Lake Bonneville, the potential hydrological and climatic linkages between the lake and glaciers are reconsidered here. Even in cases where glacier maxima occurred somewhat earlier (ie, at 20–19 ka) than the Lake Bonneville highstand, such as in the Bear River valley, Lake Bonneville was near its maximum extent during this time (Oviatt, 2015) and could have potentially affected glacier mass balance in neighboring, especially downwind, mountains.

The pattern of glacier ELAs in mountains across the northern LBB (Fig. 17.3) is especially intriguing given the correspondence of glacier maxima and the Lake Bonneville highstand at c.18 ka (Fig. 17.9). As noted earlier, the pattern of ELAs between the Ruby–East Humboldt Range in northeastern Nevada and the Wasatch Mountains does not follow the regional precipitation pattern at the mean ELA (~2750 m asl) for these mountains. If temperature depression relative to modern at ~2750 m asl in this range of latitudes was approximately uniform (ie, a function of latitude) at 18 ka, then precipitation patterns likely differed from modern. Lake Bonneville may have been a significant, local moisture source, enhancing precipitation in the Stansbury, Oquirrh, Wasatch, and western Uinta Mountains and augmenting glacier mass balance. Lake-effect storms develop over Great Salt Lake today, depositing significant snowfall in the Wasatch and western Uinta Mountains (Carpenter, 1993), and may have been greater in magnitude when the lake was larger (Hostetler et al., 1994). As noted earlier, however, this effect was likely limited in duration, as indicated by the onset of overall ice retreat at 18 ka. The fact that Lake Bonneville continued to overflow until 15 ka indicates that the water budget in the LBB remained positive, but the onset of ice

retreat suggests that climate was no longer favorable for glacier maxima. This may reflect warming at ~18 to 17 ka, but with sufficient precipitation to sustain an overflowing lake, or possibly a decline in local moisture availability for glaciers due to the 27% decline in the surface area of Lake Bonneville when it fell to the Provo shoreline (Currey et al., 1984). Given the greater sensitivity of mountain glaciers in continental interiors to temperature, ice retreat was most likely initiated by warming driven by rising summer insolation and rising atmospheric CO_2.

An alternative to the idea that Lake Bonneville enhanced precipitation delivery to glaciers in downwind mountains is that the corresponding highstand and glacier maxima represent a response to regional cooling. The Lake Bonneville highstand occurred shortly after a cooling pulse at 18.6 ka identified from a speleothem stable-isotope record from southern Nevada (Lachniet et al., 2011), suggesting that the final expansion of the lake to its highstand and corresponding occupation of terminal moraines in the LBB were driven chiefly by cooling rather than increased precipitation. This and other speleothem stable-isotope records from the southwestern United States (Asmerom et al., 2010; Wagner et al., 2010) indicate the onset of an effectively wetter climate at 18 ka or slightly later, suggesting a more complex model for temperature and precipitation changes that both sustained an overflowing Lake Bonneville and accompanied ice retreat in the LBB. Again, additional study of the pattern of ice retreat during the overflowing phase of Lake Bonneville would help to clarify the relative roles of temperature and precipitation in driving lake and glacier fluctuations during the period 18–15 ka.

17.5 SUMMARY AND CONCLUSIONS

The extent and chronology of the last glaciation in the LBB has significantly improved in recent decades due to widespread mapping efforts and the development of cosmogenic ^{10}Be and ^{3}He surface exposure dating of moraines. Mapping has enabled reconstruction of ice extents for most mountains, accounting for more than 95% of the surface area and volume of ice in the LBB during the last glaciation. The temporal correspondence of glacier maxima in the basin and the Lake Bonneville highstand is becoming clearer due to an improved understanding of the production rate of in situ ^{10}Be. Despite this improvement in the chronological framework, understanding changes in climate accompanying the later part of the transgressive phase of Lake Bonneville and the transition to the overflowing phase requires improved limits on either temperature or precipitation changes in the Great Basin. The pattern of the last glaciation as represented by mountain glacier ELAs across the northern LBB suggests enhanced precipitation in mountains engulfed by the lake and downwind of it. If such a precipitation pattern existed, it may have been limited to the brief duration of the Lake Bonneville highstand. Recent

(eg, Lachniet et al., 2011) and emerging (eg, Oster et al., 2014) speleothem records for the Great Basin and neighboring regions combined with improved chronological limits on glacial deposits could help to improve our understanding of climate change during and after the last glaciation.

ACKNOWLEDGMENTS

New cosmogenic ^{10}Be exposure ages are based on measurement of ^{10}Be/^{9}Be by M. Caffee and others at PRIME Lab and were funded by NSF/EAR-0902472. The authors thank R. Becker, E. Carson, M. Devito, D. Douglass, P. Jewell, D. Koerner, D. Marchetti, D. Mickelson, J. Moore, N. Oprandy, J. Oviatt, B. Quirk, K. Refsnider, and numerous students and field assistants for thoughtful discussions of the glacial record of the LBB.

REFERENCES

Asmerom, Y., Polyak, V.J., Burns, S.J., 2010. Variable winter moisture in the southwestern United States linked to rapid glacial climate shifts. Nat. Geosci. 3, 114–117.

Atwood, W.W., 1909. Glaciation of the Uinta and Wasatch Mountains. U.S. Geological Survey Professional Paper, 61. 96 pp.

Bahr, D.B., Meier, M.F., Peckham, S.D., 1997. The physical basis of glacier volume–area scaling. J. Geophys. Res. 102 (B9), 20355–20362.

Balco, G., Briner, J., Finkel, R.C., Rayburn, J.A., Ridge, J.C., Schaefer, J.M., 2009. Regional beryllium-10 production rate calibration for northeastern North America. Quat. Geochronol. 4, 93–107.

Balco, G., Stone, J., Lifton, N., Dunai, T., 2008. A complete and easily accessible means of calculating surface exposure ages or erosion rates from ^{10}Be and ^{26}Al measurements. Quat. Geochronol. 3, 174–195.

Benson, L.V., Lund, S.P., Smoot, J.P., Rhode, D.E., Spencer, R.J., Verosub, K.L., Louderback, L.A., Johnson, C.A., Rye, R.O., Negrini, R.M., 2011. The rise and fall of Lake Bonneville between 45 and 10.5 ka. Quat. Int. 235, 57–69.

Benson, L.V., Thompson, R.S., 1987. The physical record of lakes in the Great Basin. In: Ruddiman, W.F., Wright Jr., H.E. (Eds.), North American and Adjacent Oceans During the Last Deglaciation. Geological Society of America, vol. K-3. The Geology of North America, Boulder, CO, pp. 241–260.

Bevis, K.A., 1995. Reconstruction of late Pleistocene paleoclimatic characteristics in the Great Basin and adjacent areas (Ph.D. thesis). Oregon State University, Corvallis. 278 pp.

Blackwelder, E., 1931. Pleistocene glaciation in the Sierra Nevada and Basin Ranges. Geol. Soc. Am. Bull. 42, 865–922.

Blackwelder, E., 1915. Post-Cretaceous history of the mountains of central-western Wyoming. J. Geol. 23, 97–340.

Borchers, B., Marrero, S., Balco, G., Caffee, M., Goehring, B., Lifton, N., Nishiizumi, K., Phillips, F., Schaefer, J., Stone, J., 2016. Geological calibration of spallation production rates in the CRONUS-earth project. Quat. Geochronol. 31, 188–198. http://dx.doi.org/10.1016/j.quageo.2015.01.009.

Bracconot, P., Otto-Bliesner, B., Harrison, S., Joussaume, S., Peterchmitt, J.-Y., Abe-Ouchi, A., Crucifix, M., Driesschaert, E., Fichefet, Th., Hewitt, C.D., Kageyama, M., Kitoh, A., Laîne, A., Loutre, M.-F., Marti, O., Merkel, U., Ramstein, G., Weber, S.L., Yu, Y.,

Zhao, Y., 2007. Results of PMIP2 coupled simulations of the Mid-Holocene and Last Glacial Maximum—part 1: experiments and large-scale features. Clim. Past 3, 261–277.

Bradley, W.A., 1936. Geomorphology of the north flank of the Uinta Mountains: U.S. Geological Survey Professional Paper 185-I. pp. 163–169.

Bryant, B., 1992. Geologic and Structure Maps of the Salt Lake City 1° × 2° Quadrangle, Utah and Wyoming: U.S. Geological Survey Miscellaneous Investigations Series Map I-1997. 1:125,000 scale.

Carpenter, D.M., 1993. The lake effect of the Great Salt Lake—overview and forecast problems. Weather Forecast. 8, 181–193.

Clark, P.U., Dyke, A.S., Shakun, J.D., Carlson, A.E., Clark, J., Wohlfarth, B., Mitrovica, J.X., Hostetler, S.W., McCabe, A.M., 2009. The Last Glacial Maximum. Science 325, 710–714.

Currey, D.R., Atwood, G., Mabey, D.R., 1984. Major levels of Great Salt Lake and Lake Bonneville. Utah Geological and Mineral Survey, Map 73. .

DeGraff, J.V., Gallegos, A.J., 1983. Relative dating of glacial deposits on the northern Sevier, Fish Lake, and UM Plateaus, central Utah: abstracts with programs. Geol. Soc. Am. 15 (5), 431.

Douglass, D.C., 2000. Glacial history of the west fork of Beaver Creek, Uinta Mountains, Utah. Unpublished M.S. thesis, University of Wisconsin, Madison. 64 pp.

Foley, L.L., Martin Jr., R.A., Sullivan, J.T., 1986. Seismotectonic study for Joes Valley, Scofield, and Huntington North Dams, Emergy County and Scofield Projects, Utah: U.S. Bureau of Reclamation Seismotectonic Report No. 86-7.

Gilbert, G.K., 1890. Lake Bonneville. U. S. Geological Survey Monograph, 1. 438 pp.

Godsey, H.S., Atwood, G., Lips, E., Miller, D.M., Milligan, M., Oviatt, C.G., 2005. Don R. Currey Memorial field trip to the shores of Pleistocene Lake Bonneville. In: Pederson, J., Dehler, C.M. (Eds.), Interior Western United States. Geological Society of America Field Trip Guide, vol. 6, pp. 419–448.

Hansen, W.R., 1975. The geologic story of the Uinta Mountains. U.S. Geol. Surv. Bull. 1291, 144.

Hostetler, S.W., Giorgi, F., Bates, G.T., Bartlein, P.J., 1994. Lake-atmosphere feedbacks associated with paleolakes Bonneville and Lahontan. Science 263, 665–668.

Ives, R.L., 1950. Glaciation in Little Cottonwood Canyon. Sci. Mon. 71, 105–117.

Kaufman, D.S., 2003. Amino acid paleothermometry of quaternary ostracodes from the Bonneville basin, Utah. Quat. Sci. Rev. 22, 899–914.

Kirby, M.E., Feakins, S.J., Bonuso, N., Fantozzi, J.M., Hiner, C.A., 2013. Latest Pleistocene to Holocene hydroclimates from Lake Elsinore, California. Quat. Sci. Rev. 76, 1–15.

Laabs, B.J.C., Amidon, W.A., Munroe, J.S., 2015. Combining Numerical Modeling of Pleistocene Glaciers and Lakes to Infer Climate Change During the Last Glaciation and Deglaciation in the Northern Great Basin, Utah and Nevada, U.S.A. In: Rosen, M.R., Cohen, A.S., Kirby, M., Gierlowski-Kordesch, K., Starratt, S.W., Valero Garces, B.L., Varekamp, J. (Eds.), Abstract Volume, Sixth International Limnogeology Congress, U.S., Geological Survey Open File Report 2015-1092, pp. 123–124.

Laabs, B.J.C., Munroe, J.S., Best, L.C., Caffee, M.W., 2013. Timing of the last glaciation and subsequent deglaciation in the Ruby Mountains, Great Basin, U.S.A. Earth Planet. Sci. Lett. 361, 16–25.

Laabs, B.J.C., Marchetti, D.W., Munroe, J.S., Refsnider, K.A., Gosse, J.C., Lips, E.W., Becker, R.A., Mickelson, D.M., Singer, B.S., 2011. Chronology of latest Pleistocene mountain glaciation in the western Wasatch Mountains, Utah, U.S.A. Quat. Res. 76, 272–284.

Laabs, B.J.C., Plummer, M.A., Mickelson, D.M., 2006. Climate during the last glacial maximum in the Wasatch and southern Uinta Mountains inferred from glacier modeling. Geomorphology 75, 300–317.

Laabs, B.J.C., Refsnider, K.A., Munroe, J.S., Mickelson, D.M., Applegate, P.A., Singer, B.S., Caffee, M.W., 2009. Latest Pleistocene glacial chronology of the Uinta Mountains: support for moisture-driven asynchrony of the last deglaciation. Quat. Sci. Rev. 28, 1171–1187.

Laabs, B.J.C., Carson, E.C., 2005. Glacial geology of the southern Uinta Mountains. In: Dehler, C.M., Pederson, J.L. (Eds.), Uinta Mountain Geology, vol. 33. Utah Geological Association Publication, Salt Lake City, Utah, pp. 235–253.

Lachniet, M.S., Asmerom, Y., Polyak, V., 2011. Deglacial paleoclimate in the southwestern United States: an abrupt 18.6 ka cold event and evidence for a North Atlantic forcing of Termination I. Quat. Sci. Rev. 30, 3803–3811.

Larsen, P.R., 1996. Glacial geomorphology of a portion of the Wasatch Plateau, Central Utah (Ph.D. dissertation). University of Utah, Salt Lake City. 186 pp.

Leonard, E., 2007. Modeled patterns of late Pleistocene glacier inception and growth in the Southern and Central Rocky Mountains, USA: sensitivity to climate change and paleoclimatic implications. Quat. Sci. Rev. 26, 2152–2166.

Licciardi, J.M., Clark, P.U., Brook, E.J., Elmore, D., Sharma, P., 2004. Variable responses of western U.S. glaciers during the last deglaciation. Geology 32, 81–84.

Lifton, N., Caffee, M., Finkel, R., Marrero, S., Nishiizumi, K., Phillips, F.M., Goehring, B., Gosse, J., Stone, J., Schaefer, J., Theriault, B., Jull, A.J.T., Fifield, K., 2015. In situ cosmogenic nuclide production rate calibration for the CRONUS-earth project from Lake Bonneville, Utah, shoreline features. Quat. Geochronol. 26, 56–69.

Lifton, N.A., Phillips, F.M., Cerling, T.E., 2016. Chapter 9. Using Lake Bonneville Features to Calibrate In Situ Cosmogenic Nuclide Production Rates. In: Oviatt, C.G., Shroder Jr., J.F. (Eds.), Lake Bonneville: A Scientific Update, vol. 20. Elsevier. pp. 165–183.

Lifton, N., Sato, T., Dunai, T.J., 2014. Scaling in situ cosmogenic nuclide production rates using analytical approximations to atmospheric cosmic-ray fluxes. Earth Planet. Sci. Lett. 386, 149–160.

Lisiecki, L.E., Raymo, M.E., 2005. A Pliocene–Pleistocene stack of 57 globally distributed benthic $\delta^{18}O$ records. Paleoceanography 20, PA1003. http://dx.doi.org/10.1029/2004PA001071.

Lyle, M., Heusser, L., Ravelo, C., Yamamoto, M., Barron, J., Diffenbaugh, N.S., Herbert, T., Andreasen, D., 2012. Out of the tropics: the Pacific, Great Basin lakes, and late Pleistocene water cycle in the western United States. Science 337, 1629–1633.

Madsen, D.B., Currey, D.R., 1979. Late quaternary glacial and vegetation changes, Little Cottonwood Canyon Area, Wasatch Mountains, Utah. Quat. Res. 12, 254–270.

Marchetti, D.W., Harris, M.S., Bailey, C.M., Cerling, T.E., Bergman, S., 2011. Timing of glaciation and last glacial maximum paleoclimate estimates from the Fish Lake Plateau, Utah. Quat. Res. 75, 183–195.

Marchetti, D.W., 2007. Pleistocene glaciations in central Utah—a review. In: Willis, G.C., Hylland, M.D., Clark, D.L., Chidsey Jr., T.C. (Eds.), Central Utah—Diverse Geology of a Dynamic Landscape, vol. 36. Utah Geological Survey Publication, Salt Lake City, Utah, pp. 197–203.

Marchetti, D.W., Cerling, T.E., Lips, E.W., 2005. A glacial chronology for the Fish Creek drainage of Boulder Mountain, USA. Quat. Res. 64, 263–271.

McCoy, W.D., 1977. A reinterpretation of certain aspects of the late Quaternary glacial history of Little Cottonwood Canyon, Wasatch Mountains, Utah. Unpublished M.A. thesis, University of Utah.

McGee, D., Quade, J., Edwards, R.L., Broecker, W.S., Cheng, H., Reiners, P.W., Evenson, N., 2012. Lacustrine cave carbonates: novel archives of paleohydrologic change in the Bonneville basin (Utah, U.S.A.). Earth Planet. Sci. Lett. 351–352, 182–194.

Miller, D.M., Wahl, D.B., McGeehin, J.P., Rosario, J., Oviatt, C.G., Anderson, L., Presnetsova, L., 2015. Limiting age for the Provo shoreline of Lake Bonneville. Quat. Int. 387, 99–105. http://dx.doi.org/10.1016/j.quaint.2015.01.001.

Miller, D.M., Oviatt, C.G., McGeehin, J.P., 2013. Stratigraphy and chronology of Provo shoreline deposits and lake-level implications, late Pleistocene Lake Bonneville, eastern Great Basin, USA. Boreas 42, 342–361.

Mulvey, W.E., Currey, D.R., Lindsay, L.M.W., 1984. Southernmost occurrences of later Pleistocene glaciation in Utah: Brian Head-Signey Peaks area, Markagunt Plateau. Encyclia 61, 97–101.

Munroe, J.S., Laabs, B.J.C., 2013. Temporal correspondence between pluvial lake highstands in the southwestern US and Heinrich Event 1. J. Quat. Sci. 28, 49–58.

Munroe, J.S., Laabs, B.J.C., 2009. Glacial geology of the Uinta Mountains area, Utah and Wyoming. DVD, 1 pl., scale 1:100,000, contains GIS data and text. Utah Geological Survey Miscellaneous Publications, Salt Lake City, Utah. ISBN: 1-55791-825-2. 09-4DM.

Munroe, J.S., Laabs, B.J.C., Shakun, J.D., Singer, B.S., Mickelson, D.M., Refsnider, K.A., Caffee, M.W., 2006. Latest Pleistocene advance of alpine glaciers in the southwestern Uinta Mountains, Utah, USA: evidence for the influence of local moisture sources. Geology 34, 841–844.

Munroe, J.S., 2005. Glacial geology of the northern Uinta Mountains. In: Dehler, C.M., Pederson, J.L. (Eds.), Uinta Mountain Geology, vol. 33. Utah Geological Association Publication, Salt Lake City, Utah, pp. 215–234.

Munroe, J., Mickelson, D., 2002. Last Glacial Maximum equilibrium-line altitudes and paleoclimate, northern Uinta Mountains, Utah, U.S.A. J. Glaciol. 48, 257–266.

Murray, D.R., Locke III, W.W., 1989. Dynamics of the late Pleistocene Big Timber Glacier, Crazy Mountains, Montana, U.S.A.. J. Glaciol. 35 (120), 183–190.

Muzikar, P., Elmore, D., Granger, D.E., 2003. Accelerator mass spectrometry in geologic research. Geol. Soc. Am. Bull. 115, 643–654.

Nishiizumi, K., Imamura, M., Caffee, M.W., Southon, J.R., Finkel, R.C., McAninch, J., 2007. Absolute calibration of ^{10}Be AMS standards. Nucl. Instrum. Meth. Phys. Res. B 258, 403–413.

Osborn, G., Bevis, K., 2001. Glaciation of the Great Basin of the western United States. Quat. Sci. Rev. 20, 1377–1410.

Osborn, G.D., 1973. Quaternary geology and geomorphology of the Uinta Basin and the south flank of the Uinta Mountains, Utah. Unpublished Ph.D. dissertation, University of California, Berkeley. 266 pp.

Oster, J.L., Ibarra, D.E., Winnick, M.J., Maher, K., 2015. Steering of western storms over western North America during the Last Glacial Maximum. Nat. Geosci. 8, 201–205. http://dx.doi.org/10.1038/NGEO2365.

Oster, J.L., Kelley, N.P., Montanez, I., 2014. Tracking regional and global teleconnections recorded by North American speleothem records. Abstracts with programs. Geol. Soc. Am. 46(6). 698.

Oviatt, C.G., 2015. Chronology of Lake Bonneville, 30,000 to 10,000 yr B.P. Quat. Sci. Rev. 110, 166–171.

Oviatt, C.G., 1997. Lake Bonneville fluctuations and global climate change. Geology 25 (2), 155–158.

Oviatt, C.G., 1994. Quaternary geologic map of the upper Weber River drainage basin, Summit County, Utah. Utah Geological Survey, Map 156, scale 1:50,000.

Personius, S.F., Scott, W.E., 1992. Surficial geologic map of the Sale Lake City segment and parts of adjacent segments of the Wasatch Fault Zone, Davis, Salt Lake, and Utah Counties, Utah: U.S. Geological Survey Miscellaneous Investigations Series Map I-2106, scale 1:50,000.

Phillips, F.M., Argento, D.C., Bourlès, D.L., Caffee, M.W., Dunai, T.J., Goehring, B., Gosse, J.C., Hudons, A.M., Jull, A.J.T., Kelly, M., Lifton, N., Marrero, S.M., Nishiizumi, K., Reedy, R.C., Stone, J.O.H., 2016. Where now? Reflections on future directions for cosmogenic nuclide research from the CRONUS Projects. Quat. Geochronol. 31, 155–159. http://dx.doi.org/10.1016/j.quageo.2015.04.010.

Phillips, F.M., Zreda, M., Plummer, M.A., Elmore, D., Clark, D.H., 2009. Glacial geology and chronology of Bishop Creek and vicinity, eastern Sierra Nevada, California. GSA Bull. 121, 1013–1023.

Piegat, J.J., 1980. Glacial geology of central Nevada. Unpublished M.S. thesis, Purdue University.

Porter, S.C., Pierce, K.L., Hamilton, T.D., 1983. Late Wisconsin mountain glaciation in the western United States. In: Porter, S.C. (Ed.), Late-Quaternary environments in the western United States. The Late Pleistocene, vol. 1. University of Minnesota Press, Minneapolis, MN, pp. 71–111.

Quirk, B.J., Moore, J., Laabs, B.J.C., Caffee, M.W., Plummer, M.A., 2015. Pleistocene Glacial Chronology and Paleoclimate of Big Cottonwood Canyon, Wasatch Range, Utah. Abstract EP53A-0997, Presented at the 2015 Fall Meeting, AGU, San Francisco, CA, 14–18 December.

Radić, V., Hock, R., Oerlemans, J., 2007. Volume-area scaling vs. flowline modeling in glacier volume projections. Ann. Glaciol. 46, 234–240.

Refsnider, K.A., Laabs, B.J.C., Plummer, M.A., Mickelson, D.M., Singer, B.S., Caffee, M.W., 2008. Last glacial maximum climate inferences from cosmogenic dating and glacier modeling of the western Uinta ice field, Uinta Mountains, Utah. Quat. Res. 69, 130–144.

Refsnider, K.A., Laabs, B.J.C., Mickelson, D.M., 2007. Glacial geology of the Provo River drainage, Uinta Mountains, U.S.A.. Arct. Antarct. Alp. Res. 39, 529–536.

Reheis, M.C., Adams, K.D., Oviatt, C.G., Bacon, S.N., 2014. Pluvial lakes in the Great Basin of the western United States—a view from the outcrop. Quat. Sci. Rev. 97, 33–57.

Reheis, M.C., Laabs, B.J.C., Forester, R.M., McGeehin, J.P., Kaufman, D.S., Bright, J., 2005. Surficial deposits in the Bear Lake basin. United States Geological Survey, Open-File Report 2005–1088. 30 pp.

Richmond, G., 1964. Glaciation of Little Cottonwood and Bells Canyons, Wasatch Mountains, Utah. U.S. Geological Survey Professional Paper 454-D, D1–D41.

Richmond, G., 1965. Glaciation in the Rocky Mountains. In: Wright, H.E., Frey, D.G. (Eds.), The Quaternary of the United States. Princeton University Press, Princeton, NJ, pp. 217–230.

Richmond, G., 1957. Three pre-Wisconsin glacial stages in the Rocky Mountain region. Geol. Soc. Am. Bull. 68, 239–262.

Rosenbaum, J.G., Heil Jr., C.W., 2009. The glacial/deglacial history of sedimentation in Bear Lake, Utah and Idaho. In: Rosenbaum, J.G., Kaufman, D.S. (Eds.), Paleoenvironments of Bear Lake, Utah and Idaho, and Its Catchment. Geological Society of America Special Paper 450, Boulder, CO, pp. 247–262.

Russell, I.C., 1885. Geological history of Lake Lahontan, a Quaternary lake of northwestern Nevada. U.S. Geological Survey Monograph 11. 288 pp.

Scott, W.E., 1988. Temporal relations of lacustrine and glacial events at Little Cottonwood and Bells canyons, Utah. In: Machette, M.N. (Ed.), In the Footsteps of G.K. Gilbert; Lake Bonneville and Neotectonics of the Eastern Basin and Range Province; Guidebook for Field Trip Twelve, Utah Geological Survey Miscellaneous Publication 88–1, 78–81, Salt Lake City, UT.

Scott, W.E., Shroba, R.R., 1985. Surficial geologic map of an area along the Wasatch Fault Zone in the Salt Lake Valley, Utah. U.S. Geological Survey Open-File Report 85-448. 19 pp.

Scott, W.E., McCoy, W.D., Shroba, R.R., Rubin, M., 1983. Reinterpretation of the exposed record of the last two cycles of Lake Bonneville, western United States. Quat. Res. 20, 261–285.

Shakun, J.D., Clark, P.U., He, F., Lifton, N.A., Liu, Z., Otto-Bliesner, B.L., 2015. Regional and global forcing of glacier retreat during the last deglaciation. Nat. Commun. 6, 8059. http://dx.doi.org/10.1038/ncomms9059.

Sharp, R.P., 1938. Pleistocene Glaciation in the Ruby-East Humboldt Range, northeastern Nevada. J. Geomorphol. 1, 296–323.

Stanford, J.D., Rohling, E.J., Hunter, S.E., Roberts, A.P., Rasmussen, S.O., Bard, E., McManus, J., Fairbanks, R.G., 2006. Timing of meltwater pulse 1a and climate responses to meltwater injections. Paleoceanography 21, PA4103.

Thackray, G.D., 2008. Varied climatic and topographic influences on late Plestocene mountain glaciation in the western United States. J. Quat. Sci. 23, 671–681.

Wagner, J.D.M., Cole, J.E., Beck, J.W., Patchett, P.J., Henderson, G.M., Barnett, H.R., 2010. Moisture variability in the southwestern United States linked to abrupt glacial climate change. Nat. Geosci. 3, 110–113.

Zielinski, G.A., McCoy, W.D., 1987. Paleoclimatic implications of the relationship between modern snowpack and late Pleistocene equilibrium-line altitudes in the mountains of the Great Basin, western U.S.A. Arct. Alp. Res. 19 (2), 127–134.